The role of Rab small GTPases in recycling endosomal compartments

博 士 論 文

The role of Rab small GTPases in recycling endosomal compartments

（リサイクリングエンドソームにおける
低分子量 G 蛋白質 Rab の役割）

平成３０年度

東北大学大学院生命科学研究科

生命機能科学専攻

衞藤 貫

Contents

Overview

A recycling endosome (RE) is an organelle that functions as a sorting station of endocytic cargoes to their appropriate destinations. The endosomal sorting machinery is essential for fundamental cellular functions that underlie developmental processes. However, the precise molecular mechanisms that regulate the biogenesis and functions of REs are poorly understood. To elucidate the molecular bases of regulation and functions of REs, I focused on the small GTPase Rab, a conserved switch molecule for membrane trafficking by cycling between a GDP-bound inactive state and a GTP-bound active state. The active Rab drives a variety of membrane trafficking steps such as vesicle budding, transport, and fusion by recruiting its specific effector protein. Rab family consists of ~60 members in mammalian cells, and each Rab member is thought to regulate different intracellular membrane trafficking pathways. In this thesis, I report two mechanisms involving the regulation of REs: "The Rab35–centaurin-β2 complex regulates neurite outgrowth (Chapter 1)" and "Rab10 regulates tubular endosome formation through KIF13A/B motors (Chapter 2)".

In Chapter 1, I performed the functional analysis of Rab35 that acts as a regulator of REs during neurite outgrowth. Previous studies from our groups have shown that Rab35 regulates neurite outgrowth by recruiting several Rab35-effectors to REs. Since Rab35 was unable to bind to all Rab35-effectors simultaneously, it is reasonable to expect that Rab35 uses them as the situation demands. However, little is known about the mechanism by which Rab35 recognizes each Rab35-effector and contribution of each effector to neurite outgrowth. In this chapter, I focused on centaurin-β2 (also

called ACAP2) and attempted to identify the critical residues for the specific interaction between Rab35 and centaurin-β2 by mutation analyses. I found that two Thr residues in the switch II region of Rab35 are responsible for the binding of centaurin-β2, but not all other Rab35-effectors. Furthermore, knockdown-rescue experiments showed that a centaurin-β2-binding-deficient Rab35 mutant, Rab35(T76S/T81A), failed to support NGF-induced neurite outgrowth, indicating that Rab35–centaurin-β2 complex is necessary for neurite outgrowth.

In Chapter 2, I focused on the tubular endosome, which has recently been discovered as a novel RE distinct from a well-known transferrin receptor-positive RE. Although the tubular endosome has been characterized as a RE involving a clathrin-independent endocytic pathway, the molecular mechanism of the tubular endosome formation remains largely unknown. In the second chapter, I tried to identify essential Rabs for the tubular endosome formation and to uncover their role in tubular endosomes. First, I performed a comprehensive localization screening of the Rab subfamily and succeeded in identifying Rab10 as a novel protein predominantly localized at tubular endosomes. I also found that knockout of Rab10 completely disrupted the formation of tubular endosomes. Furthermore, I identified kinesin motors KIF13A/B as novel Rab10-interacting proteins by means of *in silico* screening and found that their knockout also disrupted tubular endosome formation. The results demonstrated that both the Rab10-binding homology domain and the motor domain of KIF13A are required for Rab10-positive tubular endosome formation.

Abbreviations

GAP: GTPase-activating protein

AA: amino acids

ACAP: ArfGAP with coiled-coil, ankyrin repeat and PH domain

ANKR: ankyrin repeat

Centβ2: centaurin-β2

CIE: clathrin-independent endocytosis

CME: clathrin-mediated endocytosis

DKO: double knockout

EE: early endosome

EGFP: enhanced green fluorescent protein

HRP: horseradish peroxidase

KO: knockout

mStr: monomeric Strawberry

NGF: nerve growth factor

PCC: Pearson's correlation coefficient

QL: Q67L

Rab35BP: Rab35-binding protein

RBD10: Rab10-binding domain

RBD35: Rab35-binding site

RE: recycling endosome

RHD10: Rab10-binding homology domain

shRNA: short hairpin RNA

siRNA: small interfering RNA

SN: S22N

SR: shRNA/siRNA-resistant

Tf: transferrin

TfR: transferrin receptor

trans-Golgi network: TGN

WT: wild-type

Chapter 1

Rab35–centaurin-β2 complex regulates neurite outgrowth

Abstract

The small GTPase Rab35 is a molecular switch for membrane trafficking that regulates a variety of cellular events. It has previously shown that Rab35 promotes neurite outgrowth of nerve growth factor-stimulated PC12 cells through interaction with centaurin-β2 (also called ACAP2). Centaurin-β2 is the only Rab35-binding protein reported thus far that exclusively recognizes Rab35 and does not recognize any of the other 59 Rabs identified in mammals, but the molecular basis for the exclusive specificity of centaurin-β2 for Rab35 has remained completely unknown. In this thesis, I performed deletion and mutation analyses and succeeded in identifying the residues of Rab35 and centaurin-β2 that are crucial for formation of a Rab35–centaurin-β2 complex. I found that two threonine residues (Thr-76 and Thr-81) in the switch II region of Rab35 are responsible for binding centaurin-β2 and that the same residues are dispensable for Rab35 recognition by other Rab35-binding proteins. I also determined the minimal Rab35-binding site (RBD35) of centaurin-β2 and identified two Asn residues (Asn-610 and Asn-691) in the RBD35 as key residues for its specific Rab35 recognition. I further showed by knockdown-rescue approaches that neither a centaurin-β2-binding-deficient Rab35(T76S/T81A) mutant nor a Rab35-binding-deficient centaurin-β2(N610A/N691A) mutant supported neurite outgrowth of PC12 cells, thereby demonstrating the functional significance of the Rab35–centaurin-β2 interaction during neurite outgrowth of PC12 cells.

Introduction

The Rab family is the largest family within the Ras superfamily of small GTPases and is conserved in all eukaryotes. The members of the Rab family are generally thought to be key players in membrane trafficking, which underlies a variety of cellular events (1–4). Rabs act as switch molecules that cycle between two nucleotide-bound states, a GTP-bound active state and a GDP-bound inactive state, and the cycling is controlled by two regulatory factors, a guanine nucleotide exchange factor (GEF), which activates Rabs, and a GTPase-activating protein (GAP), which inactivates Rabs (5, 6). The active Rabs drive various steps of membrane trafficking, including vesicle budding from donor membranes, vesicle movement along the cytoskeleton, vesicle docking to acceptor membranes, and vesicle fusion, by recruiting their specific effector molecules (1–4).

The results of recent comprehensive screenings for mammalian Rab effectors have indicated that interactions between Rabs and their effectors are more complicated than previously thought (7, 8), and most Rab isoforms appear to interact with two or more different types of effector molecules. Because mammalian cells and tissues are highly specialized, the presence of multiple Rab effectors may enable a single Rab isoform to control different types (or steps) of membrane trafficking in specialized cells. However, the physiological significance of the presence of multiple Rab effectors and their Rab recognition mechanisms are poorly understood.

Rab35 is one such Rab protein and has been shown to bind various candidate

effector molecules, including MICAL-1 (7), MICAL-L1 (7, 9, 10), MICAL-cl (7), OCRL (7, 11), RUSC2 (12), Fascin1 (13), and centaurin-β2 (8, 14), and to be involved in various cellular events, including cytokinesis (11, 15, 16), cell migration (17, 18), phagocytosis (19, 20), immunological synapse formation (21), myelination (22), and neurite outgrowth (10, 14, 23, 24), most likely through regulation of endocytic recycling (or REs) (25). The pleiotropic roles of Rab35 in membrane trafficking may be attributable to the presence of multiple Rab35 effectors, but the involvement of individual Rab35 effectors in the above cellular events has remained largely unknown. Moreover, almost nothing is known about the structural basis of Rab35–effector complexes, e.g., about the critical amino acid residues for the Rab35–effector interactions. Although identification of a specific amino acid(s) in Rab35 that is exclusively involved in interaction with only one effector molecule would enhance our understanding of the molecular mechanism of Rab35-mediated membrane trafficking, no attempts have ever been made to biochemically analyze Rab35–effector interactions.

In this thesis, I focused on centaurin-β2 (also called ACAP2, ArfGAP with coiled-coil, ankyrin repeat and PH domain), an Arf6-GAP (26) that is required for nerve growth factor (NGF)-induced neurite outgrowth of PC12 cells (8, 14), and analyzed the exclusive specificity of the Rab35–centaurin-β2 interaction with Rab35 by performing deletion and mutation analyses. The results showed that two Thr residues (Thr-76 and Thr-81) in the switch II region of Rab35 are responsible for binding centaurin-β2 and that they are not responsible for Rab35 binding to other effectors. Knockdown-rescue experiments showed that a centaurin-β2-binding-deficient Rab35 mutant,

Rab35(T76S/T81A), did not support NGF-induced neurite outgrowth. Based on my findings, I discuss the utility of the Rab35(T76S/T81A) mutant as a tool to investigate the involvement of the Rab35–centaurin-β2 complex in Rab35-dependent cellular events.

Materials and Methods

Antibodies

Horseradish peroxidase (HRP)-conjugated anti-FLAG tag (M2) mouse monoclonal antibody, anti-FLAG tag antibody-conjugated agarose (Sigma-Aldrich), HRP-conjugated anti-T7 tag mouse monoclonal antibody (Merck Biosciences Novagen, Darmstadt, Germany), anti-centaurin-β2 goat polyclonal antibody (Santa Cruz Biotechnology, Santa Cruz, CA), anti-GFP rabbit polyclonal antibody (MBL, Nagoya, Japan), and anti-β-actin mouse monoclonal antibody (Applied Biological Materials, Richmond, BC, Canada) were obtained commercially. The anti-Rab35 antibody was prepared as described previously (14).

Plasmid Construction

Mutant mouse Rab35 expression plasmids carrying a Thr-to-Ser and Thr-to-Ala double mutation at amino acid positions 76 and 81, respectively, named Rab35(T76S/T81A), a swapping mutation in the switch II region between Rab35 (amino acids (AA) 82–88) and Rab5A (AA70–76), named Rab35(S5A), see Figure 2A for details, or a small interfering RNA (siRNA)-resistant mutant, named $Rab35^{SR}$, were produced by PCR sewing methods essentially as described previously (27). In brief, PCRs were performed to generate two DNA fragments having overlapping ends into which specific alterations were introduced by using two sets of oligonucleotides, e.g., 5'-CGGATCCATGGCCCGGGACTACGACCA-3' (Rab35-Met primer, sense) and

5’-ATGGGCCCCCCGATAATAGGAAGA-3’ (Rab35-T76S/T81A-3’ primer, antisense); and 5’-TCTTCCTATTATCGGGGGGCCCAT-3’ (Rab35-T76S/T81A-5’ primer, sense) and 5’-**TTA**GCAGCAGCTTTCTTTCG-3’ (Rab35-stop primer, antisense) (substituted nucleotides are underlined, and stop codons are in bold). After purification of the two DNA fragments, they were combined to generate the fusion product by a second PCR, in which the Rab35-Met primer and Rab35-stop primer were used. The resulting Rab35 mutant cDNAs were subcloned into the pEGFP (enhanced green fluorescent protein)-C1 vector (Clontech-Takara Bio Inc., Shiga, Japan), pGBD-C1 vector (28), and pEF-FLAG tag expression vector (29). Mutant mouse centaurin-β2 fragments carrying a N610A, N632A, T648A, N691A, T695A/E697A, N724A, S730A, L733A/Y734A, Q764A/Q765A, N610A/N691A, or T648A/N691A mutation(s) were similarly produced by the method described above, and they were subcloned into the pEGFP-C1 vector, pAct2 vector (Clontech-Takara Bio Inc.), and/or pEF-T7 tag expression vector (29). Deletion mutants of centaurin-β2 (AA580–770, AA630–770, AA662–770, AA580–755, AA580–745, AA580–730, AA580–697, and AA630–730; see Figure 5A for details) were prepared by conventional PCR techniques as described previously (30). cDNAs encoding the ankyrin repeat (ANKR) domain of centaurin-β1 (Centβ1-ANKR, AA548–740) and of centaurin-β5 (Centβ5-ANKR, AA565–833), and full-length of Fascin1 were amplified by conventional PCR techniques as described previously (29) and were then subcloned into the pAct2 vector and/or pEF-T7 tag expression vector. Deletion mutants of centaurin-β2 (pAct2-Centβ2-ANKR and pEGFP-C1-Centβ2^{SR}(ΔANKR)) were prepared as described

previously (8, 14). Short hairpin RNAs (shRNAs) targeting rat *Centβ2* (shCentβ2, 19-base target site: 5'-GGGTATCTGTTCAAACGAG-3') and rat *Rab35* (shRab35 #1, 19-base target site: 5'-TATTAGTGGGCAATAAGAA-3') were also prepared as described previously (14).

Co-immunoprecipitation Assays in COS-7 Cells and Immunoblotting

T7-tagged centaurin-β2 (centaurin-β1/2/5-ANKR or Fascin1) and FLAG-tagged Rab35 (wild-type (WT), T76S/T81A, or S5A) were transiently expressed in COS-7 cells, and their associations were evaluated by co-immunoprecipitation assays with anti-FLAG tag antibody-conjugated agarose beads as described previously (29, 31). Proteins bound to the beads were analyzed by 10%, or 12.5% SDS-PAGE followed by immunoblotting with HRP-conjugated anti-T7 tag antibody (1:10,000 dilution) and HRP-conjugated anti-FLAG tag antibody (1:10,000 dilution). Immunoreactive bands were visualized by enhanced chemiluminescence (GE Healthcare Ltd.). The blots shown in this thesis are representative of at least three independent experiments.

Yeast Two-hybrid Assays

Yeast two-hybrid assays were performed by using pGBD-C1-Rab35(Q67L, Q67L/T76S/T81A, or Q67L/S5A) lacking the C-terminal geranylgeranylation site and pGAD-C1-RUSC2-RUN (12), pAct2-MICAL-1, pAct2-MICAL-cl, pAct2-MICAL-L1, pAct2-OCRL (7), pAct2-Fascin1, or pAct2-Centβ2-ANKR (8), or by using pGBD-C1-Rab35(Q67L or S22N)ΔCys (hereafter simply designated as QL or SN) and

pAct2-Centβ2-ANKR(WT or its mutants), pAct2-Centβ1-ANKR, or pAct2-Centβ5-ANKR as described previously (7, 8, 32). The yeast strain, medium, culture conditions, and transformation protocol used were as described previously (28). The assays were performed in duplicates and the results of one representative set of assays are shown.

Cell Cultures and Transfections

PC12 cell and COS-7 cell cultures and plasmid transfections were performed essentially as described previously (14). Plasmids were transfected into cultured cells 1 day after plating, by using Lipofectamine LTX or Lipofectamine 2000 (Invitrogen), each according to the manufacturer's instructions. Because the protein expression level of wild-type and mutant Rab35^{SR} (or centaurin-β2^{SR}) differs slightly even when the same amount of plasmid is transfected into PC12 cells, the amounts of plasmid used for transfection were varied (e.g., 0.04–0.1 μg of the pEGFP-C1-Rab35^{SR} plasmid and 0–0.06 μg of the pEGFP-C1 empty vector was added to keep the total amount of plasmid constant) to maintain the amount of recombinant proteins at the same level (Figures 3C and 7C). To avoid overexpression in the knockdown-rescue experiments, I tried to maintain the level of the recombinant proteins at levels that were similar to the level of the endogenous protein (Figures 3C and 7C). Under my experimental conditions, the transfection efficiency of the EGFP-expressing plasmids into PC12 cells was approximately 40–50%.

Immunofluorescence Analysis

All of the procedures used to perform the immunofluorescence analyses have been described previously (14).

Neurite Outgrowth Assays

Neurite outgrowth assays were performed essentially as described previously (14). In brief, PC12 cells that had been transfected with pSilencer plasmids together with EGFP-tagged protein-expressing plasmids were treated with 100 ng/ml β-NGF (Merck Biosciences) for 36 h. The transfected cells were identified by EGFP fluorescence and images of the cells were captured at random with a confocal fluorescence microscope (Fluoview FV1000; Olympus, Tokyo, Japan). The total neurite length of each cell (see the broken lines in Figures. 3A and 7A) was measured with MetaMorph software (Molecular Devices, Sunnyvale, CA). The results of the neurite outgrowth assays in this thesis are reported as means and SEM of data from three independent experiments (n = 100 cells; more than 30 cells were analyzed in each experiment). Because the response of PC12 cells to NGF often differs according to the number of cell passages and the lot of NGF, I used PC12 cells with a similar passage number and NGF from the same lot in any one set of experiments.

Results

Identification of Critical Residues in Rab35 for Specific Centaurin-β2 Binding by Site-directed Mutagenesis

Seven Rab35-binding proteins (Rab35BPs) have been identified thus far (7–13), but their Rab binding specificity is highly diversified, ranging from the exclusive Rab35 binding activity of centaurin-β2 (Figure 1C) to the multiple-Rab binding activity of MICAL family proteins, all of which commonly interact with Rab8A/B, Rab10, Rab13, Rab15, and Rab35, and to the even broader Rab binding activity of OCRL, which interacts with 16 Rabs (summarized in Figure 1B). In an attempt to identify the structural determinant responsible for the exclusive Rab35 binding specificity of centaurin-β2, I first focused on the switch II region of Rabs, which interact with most of the Rab35BPs (Figure 1A), because several amino acids in the switch II region of certain Rabs have previously been shown to be responsible for specific effector binding (32–38). Since Rab1A/B, Rab8A/B, Rab10, Rab13, Rab15, and Rab35 are phylogenetically similar and belong to the same large branch in the phylogenetic tree (39), the amino acid sequences of their switch II region are highly conserved. Careful inspection of their sequences, however, revealed two Thr residues, one at AA position 76 (Thr-76) and the other at AA position 81 (Thr-81), that are unique to Rab35 (arrowheads in Figure 1A). To determine whether these two Thr residues are involved in the specific recognition of Rab35 by centaurin-β2, I performed site-directed mutagenesis and generated a Rab35(T76S/T81A) mutant that carries a switch II region

of Rab1A/B (arrowheads in Figure 1A). Intriguingly, the results of the yeast-two hybrid assays showed that the T76S/T81A mutation impaired centaurin-β2 binding activity (Figure 1D, bottom panel), but had no effect on binding activity toward MICAL-1, MICAL-cl, MICAL-L1, OCRL, or RUSC2 (Figure 1D, top five panels). By contrast, I was unable to evaluate the effect of the T76S/T81A mutation on Fascin1 binding by yeast two-hybrid assays, because even the wild-type Rab35 did not interact with Fascin1 at all under my yeast two-hybrid assay conditions (Figure 1D, second panel from the bottom). To overcome this problem, I performed co-immunoprecipitation assays in COS-7 cells, and the results showed that both Rab35(WT) protein and Rab35(T76S/T81A) protein did in fact interact with Fascin1 (Figure 1E). I also investigated the impaired interaction between Rab35(T76S/T81A) and centaurin-β2 by performing co-immunoprecipitation assays in COS-7 cells. As shown in Figure 1F, the T76S/T81A mutation dramatically decreased the binding activity toward centaurin-β2, although, in contrast to the results of the yeast two-hybrid assays (Figure 1D), residual binding activity still persisted. These results indicated that both Thr-76 and Thr-81 in the switch II region of Rab35 are critical for recognition by centaurin-β2 but that they are not required for binding to other Rab35BPs.

Contribution of the Switch II Sequence in Rab35 to Binding Activity toward Rab35BPs

Next, to evaluate the contribution of the entire switch II region of Rab35 to binding activity toward Rab35BPs I produced a switch II-swapping mutant of Rab35,

named Rab35(S5A), in which the switch II region of Rab35 was replaced by the switch II region of Rab5A, a Rab that is evolutionarily distant from Rab35 (39). The results of the yeast two-hybrid assays showed that the Rab35(S5A) mutant exhibited no binding activity toward centaurin-β2 and exhibited decreased binding activity toward MICAL family members and OCRL, whereas the swapping mutation had no effect on RUSC2 binding activity (Figure 2B). To further compare the centaurin-β2 binding ability of Rab35(T76S/T81A) and Rab35(S5A), I then performed co-immunoprecipitation assays in COS-7 cells. As shown in Figure 2C, Rab35(S5A) hardly interacted with centaurin-β2 at all, in contrast to the reduced centaurin-β2 binding activity of Rab35(T76S/T81A), suggesting that centaurin-β2 recognizes certain amino acid(s) in the switch II region of Rab35 besides Thr-76 and Thr-81.

Effect of the T76S/T81A Mutation of Rab35 on NGF-induced Neurite Outgrowth of PC12 cells

Because the T76S/T81A mutation of Rab35 specifically caused a reduction in the centaurin-β2 binding activity without affecting binding activity toward other Rab35BPs (Figure 1D–E), the Rab35(T76S/T81A) mutant is expected to be a useful tool for evaluating the physiological significance of the interaction between Rab35 and centaurin-β2 by knockdown-rescue approaches. To apply the Rab35(T76S/T81A) mutant as a tool to evaluate the physiological significance of the Rab35–centaurin-β2 interaction, I focused on NGF-induced neurite outgrowth of PC12 cells, because we previously found that Rab35 recruits centaurin-β2 to Arf6-positive recycling endosomes

in PC12 cells and that knockdown of either of them with specific shRNAs inhibits neurite outgrowth (14) (Figure 3A, upper panels, and 3B). When I re-expressed an shRNA-resistant form of Rab35(WT) (named Rab35^{SR}(WT)) in Rab35-knockdown cells, NGF-induced neurite outgrowth was almost completely restored (Figure 3A, bottom left panel, and 3B), whereas re-expression of Rab35^{SR}(T76S/T81A) in Rab35-knockdown cells failed to rescue the phenotype (Figure 3A, bottom middle panel, and 3B), indicating that the specific interaction between Rab35 and centaurin-β2 is crucial for neurite outgrowth. Similarly, no rescue effect was observed with Rab35^{SR}(S5A) (Figure 3A, bottom right panel, and 3B), which also lacks centaurin-β2 binding activity (Figure 2B and 2C). The lack of a rescue effect by these two mutants is unlikely to be attributable to their lower protein expression level, because equivalent amount of Rab35^{SR} proteins were expressed under my experimental conditions (Figure 3C). Although the difference was not statistically significant, the Rab35^{SR}(T76S/T81A)-re-expressing cells tended to possess slightly longer neurites than the Rab35^{SR}(S5A)-re-expressing cells. This difference may be explained by the residual centaurin-β2 binding activity of Rab35(T76S/T81A) as opposed to the almost completely absent centaurin-β2 binding activity of Rab35(S5A) (Figure 2C), or Rab35(T76S/T81A) may weakly promote neurite outgrowth through interaction with other Rab35BPs, e.g., MICAL-L1 (10).

Rab35 Binding Activity of Centaurin-β1/ACAP1 and Centaurin-β5/ACAP3

In the next set of experiments, I turned my attention to centaurin-β2 and attempted

to identify the residues that are crucial for Rab35 binding activity. Although we previously showed that a C-terminal ANKR domain of centaurin-β2 functions as a Rab35 effector domain (8, 14), nothing was known about its Rab35 recognition mechanism. To identify the critical residues in the ANKR domain of centaurin-β2 that are responsible for Rab35 binding, I first compared the ANKR domain of ORP1L (i.e., Rab7-binding site) (40) and ANKR domain of VARP (i.e., Rab32/38-binding site) (32, 41) with the centaurin-β2 ANKR domain. Because of their low sequence conservation, however, I was unable to identify shared key residues that are responsible for Rab binding by these three ANKR domains. I then turned my attention to Arf-GAPs, because approximately two thirds of mammalian Arf-GAPs contain ANKR domains, and because two of them (42, 43), centaurin-β1 (also called ACAP1) and centaurin-β5 (also called ACAP3), contain a C-terminal ANKR domain similar to the centaurin-β2 ANKR domain (Figure 4A). If the ANKR domain of centaurin-β1/β5 also serves as a Rab35-binding site, comparison of their sequence was expected to be helpful in identifying key residues responsible for Rab35 binding. To determine whether centaurin-β1 and centaurin-β5 are binding partners of Rab35, I cloned the cDNAs of the mouse ANKR domains of centaurin-β1/β5 (Figure 4A) and subjected them to yeast two-hybrid assays as described above (Figure 4B). To my surprise, however, neither the ANKR domain of centaurin-β1 nor the ANKR domain of centaurin-β5 interacted with Rab35, despite their relatively high sequence similarity to the ANKR domain of centaurin-β2, which recognizes a GTP-locked (Q67L = QL) form of Rab35, but not its GDP-locked (S22N = SN) form. I confirmed the lack of interaction between Rab35

and centaurin-β1/β5 by performing co-immunoprecipitation assays in COS-7 cells (Figure 4C). These results suggested that amino acid residues in the centaurin-β2 ANKR domain that are not conserved in centaurin-β1 or centaurin-β5 were good candidates for key residues responsible for Rab35 binding. Because the original centaurin-β2-ANKR construct contains another regions besides the ANKR domain (Figure 4A), I wanted to reduce the Rab35-binding region to a minimum before searching for the candidate residues by sequence comparisons between the C-terminal domains of centaurin-β1, -β2, and -β5.

Determination of the Minimal Rab35-binding Site in Centaurin-β2

To determine the minimal Rab35-binding site (named RBD35), I generated a series of deletion mutants (summarized in Figure 5A) and evaluated their Rab35 binding activity by yeast two-hybrid assays. The results showed that only the AA580–755 construct strongly interacted with Rab35(QL), the same as the original ANKR construct (AA580–770) did (Figure 5B), whereas the other deletion constructs did not interact or hardly interacted with Rab35(QL). Similar results were obtained by co-immunoprecipitation assays in COS-7 cells: deletion of C-terminal 15 amino acids from the original ANKR construct (i.e., AA580–755) had no effect on Rab35 binding activity, whereas deletion of C-terminal 30 amino acids (i.e., AA580–745) impaired Rab35 binding activity (Figure 5C). I therefore concluded that the minimal RBD35 in centaurin-β2 is AA580-755 and that additional amino acids in the C-terminal flanking region of the ANKR domain, i.e., AA730-755, are required for high-affinity Rab35

binding.

Identification of Critical Residues in the ANKR Domain of Centaurin-β2 That Specifically Recognize Rab35 by Site-directed Mutagenesis

Based on the results shown in Figure 5B, I searched for candidate residues responsible for Rab35 binding in the minimal RBD35 of centaurin-β2 by performing sequence comparisons between centaurin-β1, -β2, and -β5 (Figure 6A). The 12 candidate residues conserved in centaurin-β2 alone, i.e., Asn-610, Asn-632, Thr-648, Asn-691, Thr-695, Glu-697, Asn-724, Ser-730, Leu-733, Tyr-734, Gln-764, and Gln-765, were selected, and each was replaced with Ala by site-directed mutagenesis (arrowheads in Figure 6A). The results of the yeast two-hybrid assays showed that none of the single point mutations dramatically decreased binding activity toward Rab35(QL) (Figure 6B). However, since the yeast cells expressing the N610A, T648A, or N691A mutant appeared to grow slowly, I generated double mutants of centaurin-β2, i.e., N610A/N691A and T648A/N691A, and assessed their Rab35 binding activity by yeast two-hybrid assays. As shown in Figure 6C, the N610A/N691A double mutant abrogated binding activity toward Rab35(QL), whereas the T648A/N691A double mutant still exhibited significant Rab35 binding activity. Similar results were obtained by co-immunoprecipitation assays in COS-7 cells, that is, the Rab35 binding activity of centaurin-β2(N610A/N691A) mutant was dramatically reduced (lane 2 in the middle panel of Figure 6D). These results indicated that both Asn-610 and Asn-691 in the ANKR domain of centaurin-β2 are critical for recognition

by Rab35, and I decided to use the N610A/N691A mutant as a Rab35-binding-deficient mutant in the subsequent analysis.

Effect of the N610A/N691A Mutation of Centaurin-β2 on NGF-induced Neurite Outgrowth of PC12 cells

To investigate whether the centaurin-β2(N610A/N691A) mutant is capable of supporting NGF-induced neurite outgrowth, I performed knockdown-rescue experiments as described previously (14). Consistent with our previous finding, knockdown of centaurin-β2 with specific shRNA inhibited neurite outgrowth (Figure 7A, upper panels, and 7B), whereas re-expression of centaurin-β2^{SR}(WT) in centaurin-β2-knockdown cells rescued the phenotype (14) (Figure 7A, bottom left panel, and 7B). By contrast, re-expression of centaurin-β2^{SR}(N610A/N691A) in centaurin-β2-knockdown cells failed to rescue the phenotype (Figure 7A, bottom middle panel, and 7B), the same as the centaurin-β2^{SR}(ΔANKR) mutant, which completely lacked the RBD35 (14) (Figure 7A, bottom right panel, and 7B). The lack of a rescue effect by these two mutants is unlikely to be attributable to their lower protein expression level, because equivalent amounts of centaurin-β2^{SR} proteins were expressed in the centaurin-β2-knockdown cells (Figure 7C). These results taken together indicated that the Rab35–centaurin-β2 interaction is essential for neurite outgrowth.

Discussion

We and others have previously identified a variety of Rab35BPs (7–13), each of which showed extremely different Rab binding specificity (Figure 1B). Only one of them, centaurin-β2, had been shown to specifically recognize Rab35 (Figure 1C) (8), but the molecular determinant(s) responsible for the exclusive Rab35 binding specificity of centaurin-β2 had never been investigated. In the present thesis, I performed site-directed mutagenesis and identified residues in Rab35, i.e., Thr-76 and Thr-81 in the switch II region, and in centaurin-β2, i.e., Asn-610 and Asn-691 in the ANKR domain, that are crucial for the formation of the Rab35–centaurin-β2 complex (Figures 1 and 6). Because Rab35 is the only Rab isoform that has a Thr residue at each of these positions in the switch II region (Figure 1A), centaurin-β2 is likely to specifically recognize these two Thr residues. Actually, mutation of these Thr residues resulted in a dramatic reduction in the centaurin-β2 binding ability without affecting binding activity toward any of the other Rab35BPs (Figure 1D–F). However, these results do not mean that other Rab35BPs besides centaurin-β2 recognize the switch II region of Rab35. A switch II-swapping analysis indicated that the switch II region of Rab35 also contributes to its recognition by most of the Rab35BPs (Figure 2). Because RUSC2 normally bound to the Rab35(S5A) mutant, it must recognize some other region of Rab35 besides the switch II region, suggesting that Rab35 interacts with both RUSC2 and one of the other Rab35BPs. Further work will be necessary to determine whether Rab35 actually interacts with more than one Rab35BP at the same time.

Identification of the minimal Rab35-binding site (RBD35) in centaurin-β2 provided other important information. I previously thought that the ANKR domain of centaurin-β2 was necessary and sufficient for Rab35 binding activity, the same as the ANKR1 domain of Varp alone recognizes Rab32/38 (32), but the results of my deletion analysis indicated that an N-terminal flanking region and C-terminal flanking region (AA580–630 and AA730–755, respectively) of the ANKR domain are also required for high-affinity Rab35 binding activity (Figure 5). This observation may well explain why other Arf-GAPs, e.g., centaurin-β1/5, which often have an ANKR domain (42, 43), do not interact with Rab35, because the N-terminal and C-terminal flanking regions of the ANKR domain are not well conserved among Arf-GAPs. A more detailed structural analysis will be needed to evaluate the contribution of the N/C-terminal flanking regions of the ANKR domain to Rab35 binding.

The fact that more than one Rab35BP is simultaneously expressed in a single cell type (10, 14) makes it difficult to determine which Rab35 effector is involved in Rab35-dependent cellular events. Knockdown of a certain Rab35BP is insufficient to show whether a direct interaction between Rab35 and that Rab35BP is involved in cellular events, even when the Rab35BP knockdown impairs them. The $Rab35^{SR}$(T76S/T81A) mutant that I developed in this thesis on the other hand, is a useful tool for evaluating the functional significance of the Rab35–centaurin-β2 interaction in cellular events. By using this tool in combination with knockdown-rescue approaches, I succeeded in confirming our previous finding that the interaction between Rab35 and centaurin-β2 is essential for neurite outgrowth of PC12

cells, because the centaurin-β2-binding-deficient Rab35^{SR}(T76S/T81A) mutant did not support NGF-induced neurite outgrowth of Rab35-knockdown cells (Figure 3). Similarly, the Rab35-binding-deficient centaurin-β2^{SR}(N610A/N691A) mutant was unable to restore neurite outgrowth of centaurin-β2-knockdown cells (Figure 7).

In conclusion, I performed structure-function analyses of Rab35 and centaurin-β2 by site-directed mutagenesis and identified residues that are crucial for the Rab35–centaurin-β2 interaction. I also showed by knockdown-rescue experiments that centaurin-β2 functions as a Rab35 effector during NGF-induced neurite outgrowth of PC12 cells. The Rab35^{SR}(T76S/T81A) mutant that I developed should be a powerful, easy-to-use tool for probing involvement of centaurin-β2 in Rab35-dependent cellular events, including in cell migration (18) and phagocytosis (19), at the cellular level. Actually, it has recently been shown by this mutant that the Rab35–centaurin-β2 interaction is required for podocalyxin trafficking to the apical membrane of a 2-dimensional MDCK monolayer (48).

References

1. Fukuda, M. (2008) Regulation of secretory vesicle traffic by Rab small GTPases. *Cell. Mol. Life Sci.* **65**, 2801–2813

2. Stenmark, H. (2009) Rab GTPases as coordinators of vesicle traffic. *Nat. Rev. Mol. Cell Biol.* **10**, 513–525

3. Pfeffer, S. R. (2013) Rab GTPase regulation of membrane identity. *Curr. Opin. Cell Biol.* **25**, 414–419

4. Barr, F. A. (2013) Rab GTPases and membrane identity: causal or inconsequential? *J. Cell Biol.* **202**, 191–199

5. Barr, F., and Lambright, D. G. (2010) Rab GEFs and GAPs. *Curr. Opin. Cell Biol.* **22**, 461–470

6. Fukuda, M. (2011) TBC proteins: GAPs for mammalian small GTPase Rab? *Biosci. Rep.* **31**, 159–168

7. Fukuda, M., Kanno, E., Ishibashi, K., and Itoh, T. (2008) Large scale screening for novel Rab effectors reveals unexpected broad Rab binding specificity. *Mol. Cell. Proteomics* **7**, 1031–1042

8. Kanno, E., Ishibashi, K., Kobayashi, H., Matsui, T., Ohbayashi, N., and Fukuda, M. (2010) Comprehensive screening for novel Rab-binding proteins by GST pull-down assay using 60 different mammalian Rabs. *Traffic* **11**, 491–507

9. Rahajeng, J., Giridharan, S. S. P., Cai, B., Naslavsky, N., and Caplan, S. (2012) MICAL-L1 is a tubular endosomal membrane hub that connects Rab35 and Arf6 with Rab8a. *Traffic* **13**, 82–93

10. Kobayashi, H., and Fukuda, M. (2013) Rab35 establishes the EHD1-association site by coordinating two distinct effectors during neurite outgrowth. *J. Cell Sci.* **126**, 2424–2435

11. Dambournet, D., Machicoane, M., Chesneau, L., Sachse, M., Rocancourt, M., Marjou, A. E., Formstecher, E., Salomon, R., Goud, B., and Echard, A. (2011) Rab35 GTPase and OCRL phosphatase remodel lipids and F-actin for successful cytokinesis. *Nat. Cell Biol.* **13**, 981–988

12. Fukuda, M., Kobayashi, H., Ishibashi, K., and Ohbayashi, N. (2011) Genome-wide investigation of the Rab binding activity of RUN domains: development of a novel tool that specifically traps GTP-Rab35. *Cell Struct. Funct.* **36**, 155–170

13. Zhang, J., Fonovic, M., Suyama, K., Bogyo, M., and Scott, M. P. (2009) Rab35 controls actin bundling by recruiting fascin as an effector protein. *Science* **325**, 1250–1254

14. Kobayashi, H., and Fukuda, M. (2012) Rab35 regulates Arf6 activity through centaurin-β2 (ACAP2) during neurite outgrowth. *J. Cell Sci.* **125**, 2235–2243

15. Kouranti, I., Sachse, M., Arouche, N., Goud, B., and Echard, A. (2006) Rab35 regulates an endocytic recycling pathway essential for the terminal steps of cytokinesis. *Curr. Biol.* **16**, 1719–1725

16. Chesneau, L., Dambouret, D., Machicoane, M., Kouranti, I., Fukuda, M., Goud, B., and Echard, A. (2012) An ARF6/Rab35 GTPase cascade for endocytic recycling and successful cytokinesis. *Curr. Biol.* **22**, 147–153

17. Allaire, P. D., Sadr, M. S., Chaineau, M., Sadr, E. S., Konefal, S., Fotouhi, M., Maret, D., Ritter, B., Maestro, R. F. D., and McPherson, P. S. (2012) Interplay between Rab35 and Arf6 controls cargo recycling to coordinate cell adhesion and migration. *J. Cell Sci.* **126**, 722–731

18. Zhu, Y., Shen, T., Liu, J., Zheng, J., Zhang, Y., Xu, R., Sun, C., Du, J., Chen, Y., and Gu, L. (2013) Rab35 is required for Wnt5a/Dvl2-induced Rac1 activation and cell migration in MCF-7 breast cancer cells. *Cell Signal.* **25**, 1075–1085

19. Shim, J., Lee, S. M., Lee, M. S., Yoon, J., Kweon, H. S., and Kim, Y. J. (2010) Rab35 mediates transport of Cdc42 and Rac1 to the plasma membrane during phagocytosis. *Mol. Cell. Biol.* **30**, 1421–1433

20. Egami, Y., Fukuda, M., and Araki, N. (2011) Rab35 regulates phagosome formation through recruitment of ACAP2 in macrophages during FcγR-mediated phagocytosis. *J. Cell Sci.* **124**, 3557–3567

21. Patino-Lopez, G., Dong, X., Ben-Aissa, K., Bernot, K. M., Itoh, T., Fukuda, M., Kruhlak, M. J., Samelson, L. E., and Shaw, S. (2008) Rab35 and its GAP EPI64C in T cells regulate receptor recycling and immunological synapse formation. *J. Biol. Chem.* **283**, 18323–18330

22. Miyamoto, Y., Yamamori, N., Torii, T., Tanoue, A., and Yamauchi, J. (2014) Rab35, acting through ACAP2 switching off Arf6, negatively regulates oligodendrocyte differentiation and myelination. *Mol. Biol. Cell* **25**, 1532–1542

23. Chevallier, J., Koop, C., Srivastava, A., Petrie, R. J., Lamarche-Vane, N., and Presley JF. (2009) Rab35 regulates neurite outgrowth and cell shape. *FEBS Lett.* **583**, 1096–1101

24. Kobayashi, H., Etoh, K., Ohbayashi, N., and Fukuda, M. (2014) Rab35 promotes the recruitment of Rab8, Rab13 and Rab36 to recycling endosomes through MICAL-L1 during neurite outgrowth. *Biol. Open* **3**, 803–814

25. Grant, B. D. and Donaldson, J. G. (2009) Pathways and mechanisms of endocytic recycling. *Nat. Rev. Mol. Cell Biol.* **10**, 597–608.

26. Jackson, T. R., Brown, F. D., Nie, Z., Miura, K., Foroni, L., Sun, J., Hsu, V. W., Donaldson, J. G., and Randazzo, P. A. (2000) ACAPs are arf6 GTPase-activating proteins that function in the cell periphery. *J. Cell Biol.* **151**, 627–638

27. Ho, S. N., Hunt, H. D., Horton, R. M., Pullen, J. K., and Pease, L. R. (1989) Site-directed mutagenesis by overlap extension using the polymerase chain reaction. *Gene* **77**, 51–59

28. James, P., Halladay, J., and Craig, E. A. (1996) Genomic libraries and a host strain designed for highly efficient two-hybrid selection in yeast. *Genetics* **144**, 1425–1436

29. Fukuda, M., Kanno, E., and Mikoshiba, K. (1999) Conserved N-terminal cysteine

motif is essential for homo- and heterodimer formation of synaptotagmins III, V, VI, and X. *J. Biol. Chem.* **274**, 31421–31427

30. Fukuda, M., Kojima, T., Aruga, J., Niinobe, M., and Mikoshiba, K. (1995) Functional diversity of C2 domains of synaptotagmin family: mutational analysis of inositol high polyphosphate binding domain. *J. Biol. Chem.* **270**, 26523–26527

31. Fukuda, M., and Kanno, E. (2005) Analysis of the role of Rab27 effector Slp4-a/granuphilin-a in dense-core vesicle exocytosis. *Methods Enzymol.* **403**, 445-457

32. Tamura, K., Ohbayashi, N., Maruta, Y., Kanno, E., Itoh, T., and Fukuda, M. (2009) Varp is a novel Rab32/38-binding protein that regulates Tyrp1 trafficking in melanocytes. *Mol. Biol. Cell* **20**, 2900–2908

33. Eathiraj, S., Pan, X., Ritacco, C., and Lambright, D. G. (2005) Structural basis of family-wide Rab GTPase recognition by rabenosyn-5. *Nature* **436**, 415–419

34. Recacha, R., Boulet, A., Jollivet, F., Monier, S., Houdusse, A., Goud, B., and Khan, A. R. (2009) Structural basis for recruitment of Rab6-interacting protein 1 to Golgi via a RUN domain. *Structure* **17**, 21–30

35. Eathirai, S., Mishra, A., Prekeris, R., and Lambright, D. G. (2006) Structural basis for Rab11-mediated recruitment of FIP3 to recycling endosomes. *J. Mol. Biol.* **364**, 121–135

36. Kukimoto-Niino, M., Sakamoto, A., Kanno, E., Hanawa-Suetsugu, K., Terada, T., Shirouzu, M., Fukuda, M., and Yokoyama, S. (2008) Structural basis for the exclusive specificity of Slac2-a/melanophilin for the Rab27 GTPases. *Structure* **16**, 1478–1490

37. Fukuda, M. (2002) Synaptotagmin-like protein (Slp) homology domain 1 of Slac2-a/melanophilin is a critical determinant of GTP-dependent specific binding to Rab27A. *J. Biol. Chem.* **277**, 40118–40124

38. Matsui, T., Ohbayashi, N., and Fukuda, M. (2012) The Rab interacting lysosomal protein (RILP) homology domain functions as a novel effector domain for small

GTPase Rab36: Rab36 regulates retrograde melanosome transport in melanocytes. *J. Biol. Chem.* **287**, 28619–28631

39. Pereira-Leal, J. B., and Seabra, M. C. (2001) Evolution of the Rab family of small GTP-binding proteins. *J. Mol. Biol.* **313**, 889–901

40. Johansson, M., Rocha, N., Zwart, W., Jordens, I., Janssen, L., Kuijl, C., Olkkonen, V. M., and Neefjes, J. (2007) Activation of endosomal dynein motors by stepwise assembly of Rab7–RILP–p150^{Glued}, ORP1L, and the receptor βIII spectrin. *J. Cell Biol.* **176**, 459–471

41. Hesketh, G. G., Pérez-Dorado, I., Jackson, L. P., Wartosch, L., Schäfer, I. B., Gray, S. R., McCoy, A. J., Zeldin, O. B., Garman, E. F., Harbour, M. E., Evans, P. R., Seaman, M. N., Luzio, J. P., and Owen, D. J. (2014) VARP is recruited on to endosomes by direct interaction with retromer, where together they function in export to the cell surface. *Dev. Cell* **29**, 591–606

42. Inoue, H., and Randazzo, P. A. (2007) Arf GAPs and their interacting proteins. *Traffic* **8**, 1465–1475

43. Kahn, R. A., Bruford, E., Inoue, H., Logsdon, J. M., Jr., Nie, Z., Premont, R. T., Randazzo, P. A., Satake, M., Theibert, A. B., Zapp, M. L., and Cassel, D. (2008) Consensus nomenclature for the human ArfGAP domain-containing proteins. *J. Cell Biol.* **182**, 1039–1044

44. Fujiwara, T., Bandi, M., Nitta, M., Ivanova, E. V., Bronson, R. T., and Pellman, D. (2005) Cytokinesis failure generating teraploids promotes tumorigenesis in *p53*-null cells. *Nature* **437**, 1043–1047

45. Patino-Lopez, G., Dong, X., Ben-Aissa, K., Bernot, K. M., Itoh, T., Fukuda, M., Kruhlak, M. J., Samelson, L. E., and Shaw, S. (2008) Rab35 and its GAP EPI64C in T cells regulate receptor recycling and immunological synapse formation. *J. Biol. Chem.* **283**, 18323–18330

46. Ishibashi, K., Kanno, E., Itoh, T., and Fukuda, M. (2009) Identification and characterization of a novel Tre-2/Bub2/Cdc16 (TBC) protein that possesses Rab3A-GAP activity. *Genes Cells* **14**, 41–52

47. Hsu, C., Morohashi, Y., Yoshimura, S., Manrique-Hoyos, N., Jung, S., Lauterbach, M. A., Bakhti, M., Grønborg, M., Möbius, W., Rhee, J., Barr, F. A., and Simons, M. (2010) Regulation of exosome secretion by Rab35 and its GTPase-activating proteins TBC1D10A-C. *J Cell Biol*. **189**, 223–232

48. Mrozowska, P. S., and Fukuda, M. (2016) Regulation of podocalyxin trafficking by Rab small GTPases in 2D and 3D epithelial cell cultures. *J. Cell Biol.* **213**, 355–69

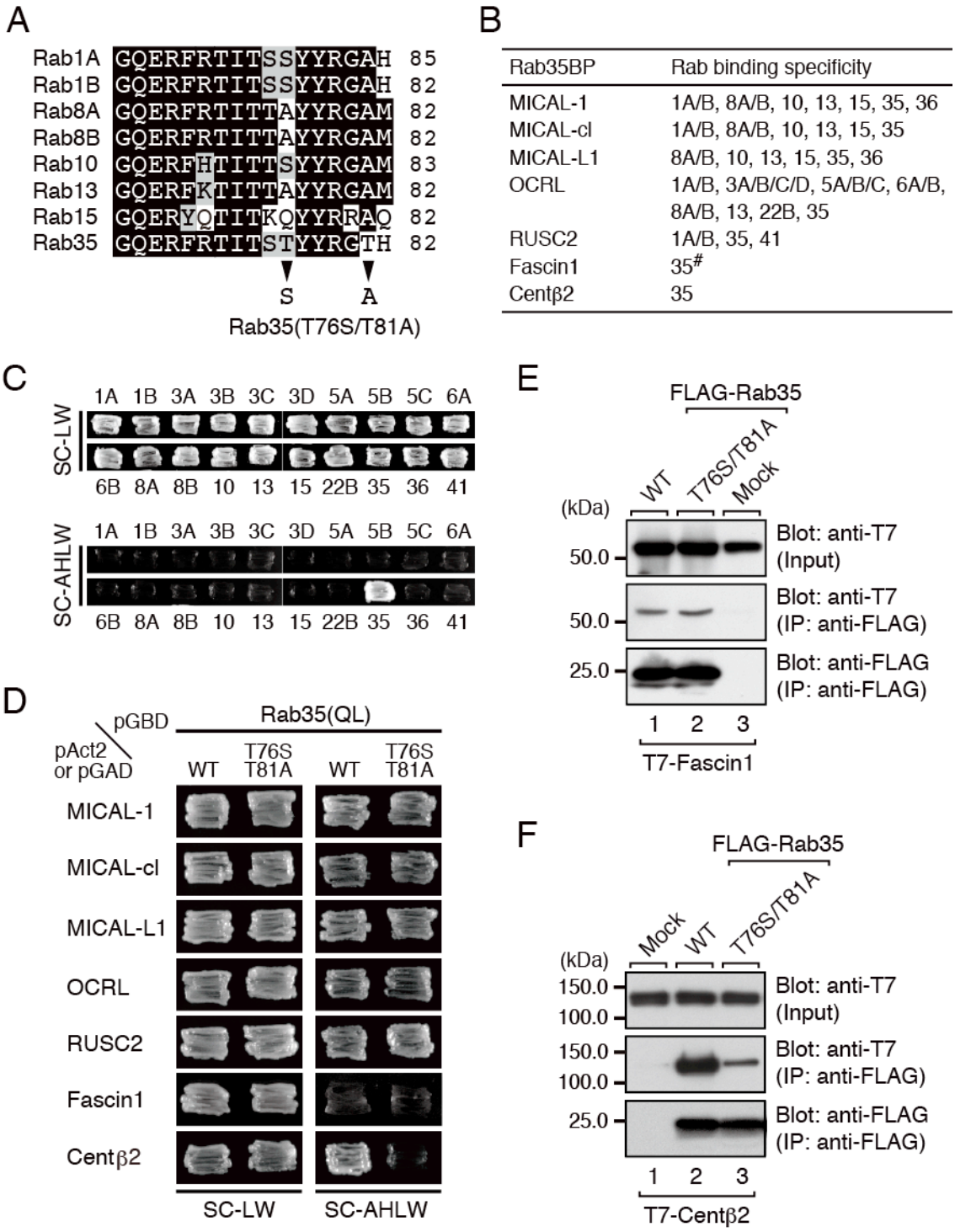

FIGURE 1. Identification of critical residues responsible for the specific binding of centaurin-β2 in the switch II region of Rab35 by site-directed mutagenesis.

(A) Sequence alignment of the switch II regions of mouse Rab1A/B, Rab8A/B, Rab10, Rab13, Rab15, and Rab35. Amino acid residues in the sequences that are conserved in

more than four switch II regions and that are similar are shown against a black background and a shaded background, respectively. Only two amino acids (arrowheads) in the switch II region of Rab1A/B and Rab35 are different, and I replaced the Thr-76 and Thr-81 of Rab35 with Ser and Ala, respectively, by site-directed mutagenesis (i.e., produced a T76S/T81A mutant, which mimics the switch II region of Rab1A).

(B) Summary of Rab35-binding proteins (Rab35BP) and their Rab-binding specificity. The Rab-binding specificity of all of the Rab35BPs except Fascin1 (#) has already been thoroughly investigated by yeast two-hybrid assays (7, 8, 12).

(C) Centaurin-β2 specifically recognized Rab35, but did not recognize other Rabs that interact with MICALs, OCRL, and RUSC2. Yeast cells containing pAct2-cenaurin-β2-ANKR and pGBD-C1-Rabs(QL)ΔCys (7) were streaked on SC-LW (top panels) and SC-AHLW (selection medium; bottom panels) and incubated at 30°C for one day and one week, respectively.

(D) Two Thr residues of Rab35, Thr-76 and Thr-81, are critical for binding centaurin-β2, but not for binding other Rab35BPs. Yeast cells containing the pAct2 (or pGAD) plasmid expressing Rab35BP and pGBD plasmid expressing the constitutive active form (Rab35(QL)) of Rab35(WT) (wild-type) or Rab35(T76S/T81A) mutant were streaked on SC-LW (left panels) and SC-AHLW (right panels) and incubated at 30°C for one day and one week, respectively.

(E) The T76S/T81A mutation did not impair Facsin1 binding activity in co-immunoprecipitation assays. T7-tagged Facsin1 and FLAG-tagged Rab35(WT) or Rab35(T76S/T81A) mutant were co-expressed in COS-7 cells, and their associations were analyzed by co-immunoprecipitation assays with anti-FLAG tag antibody-conjugated agarose beads as described previously (29, 31). Co-immunoprecipitated T7-tagged Facsin1 (middle panel) and immunoprecipitated FLAG-tagged Rab35(WT) or Rab35(T76S/T81A) mutant (bottom panel) were detected with HRP-conjugated anti-T7 tag antibody and HRP-conjugated anti-FLAG tag antibody, respectively. The positions of the molecular mass markers (in kilodaltons) are shown on the left.

(F) The T76S/T81A mutation dramatically decreased the centaurin-β2 binding activity of Rab35, a finding that was consistent with the results of the yeast two-hybrid assays shown in D. Co-immunoprecipitation assays were performed as described in E.

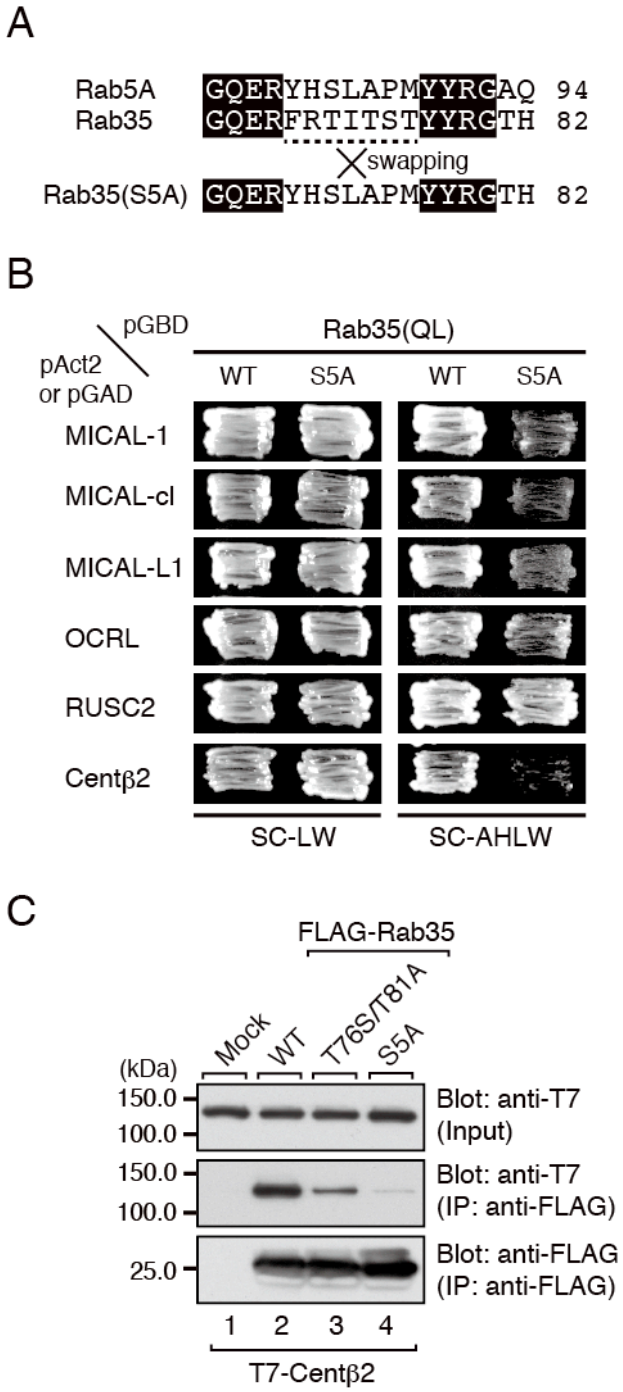

FIGURE 2. Involvement of the switch II region of Rab35 in the binding of Rab35BPs.

(A) Sequence alignment of the switch II regions of mouse Rab5A and Rab35. Amino acid residues that are conserved in the two sequences are shown against a black

background. The central parts of their switch II region (dashed line) were swapped, and the Rab35(S5A) mutant contains part of the switch II region of Rab5A.

(B) The switch II region of Rab35 is required for binding all Rab35BPs except RUSC2. Yeast two-hybrid assays were performed as described in the legend for Figure 1C.

(C) The Rab35(S5A) mutant hardly interacted with centaurin-β2 at all, in contrast to the weak centaurin-β2 binding activity of the Rab35(T76S/T81A) mutant. Co-immunoprecipitation assays were performed as described in the legend for Figure 1E. The positions of the molecular mass markers (in kilodaltons) are shown on the left.

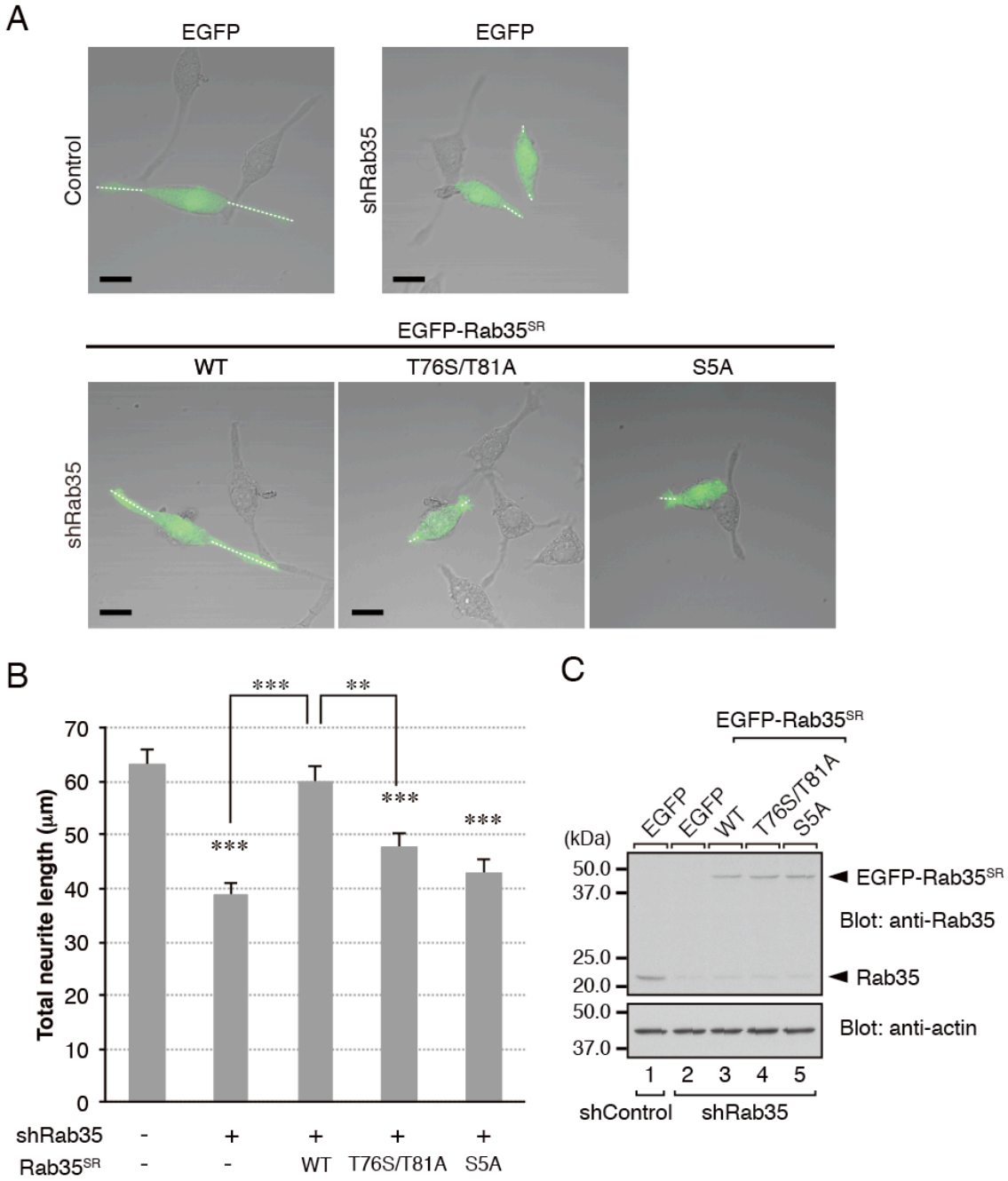

FIGURE 3. Effect of the T76S/T81A mutation of Rab35 on NGF-induced neurite outgrowth of PC12 cells.

(A) Typical images of PC12 cells (merged bright-field images and EGFP fluorescence images) transiently expressing shControl or shRab35 together with pEGFP-C1 (top row) or together with pEGFP-C1-Rab35^{SR}(WT, T76S/T81A, or S5A) (bottom row). The cells were fixed after NGF stimulation for 36 h and examined under a confocal microscope. Under my experimental conditions, manipulation of Rab35 had no

significant effect on the number of neurites (shControl, 2.2 ± 0.06; shRab35, 2.0 ± 0.04; shRab35 + Rab35^{SR}(WT), 2.3 ± 0.06; shRab35 + Rab35^{SR}(T76S/Y81A), 2.1 ± 0.05; and shRab35 + Rab35^{SR}(S5A), 1.9 ± 0.05 (mean ± SEM)), suggesting that Rab35 is involved in neurite extension rather than in neuritogenesis. Scale bars, 20 μm.

(B) Quantification of total neurite length shown in A (sum of the lengths of the broken white lines in each PC12 cell). The bars represent the means and SEM of data from three independent experiments (n = 100 cells; more than 30 cells were analyzed in each experiment). **, $p < 0.01$; ***, $p < 0.001$ (one-way ANOVA followed by the Tukey-Kramer test). In contrast to the typical Rab35-knockdown cells shown in A, some EGFP-positive Rab35-knockdown cells still had longer neurites, presumably because of low knockdown efficiency, and the mean total neurite length of the Rab35-knockdown cells appeared to be overestimated.

(C) Equivalent expression level of EGFP-Rab35^{SR}(WT, T76S/T81A, or S5A) in shRab35-expressing PC12 cells. Cell lysates of PC12 cells expressing shRab35 together with EGFP-Rab35^{SR}(WT, T76S/T81A, or S5A) were subjected to 12.5% SDS-PAGE followed by immunoblotting with anti-Rab35 antibody and anti-actin antibody. The positions of the molecular mass markers (in kilodaltons) are shown on the left.

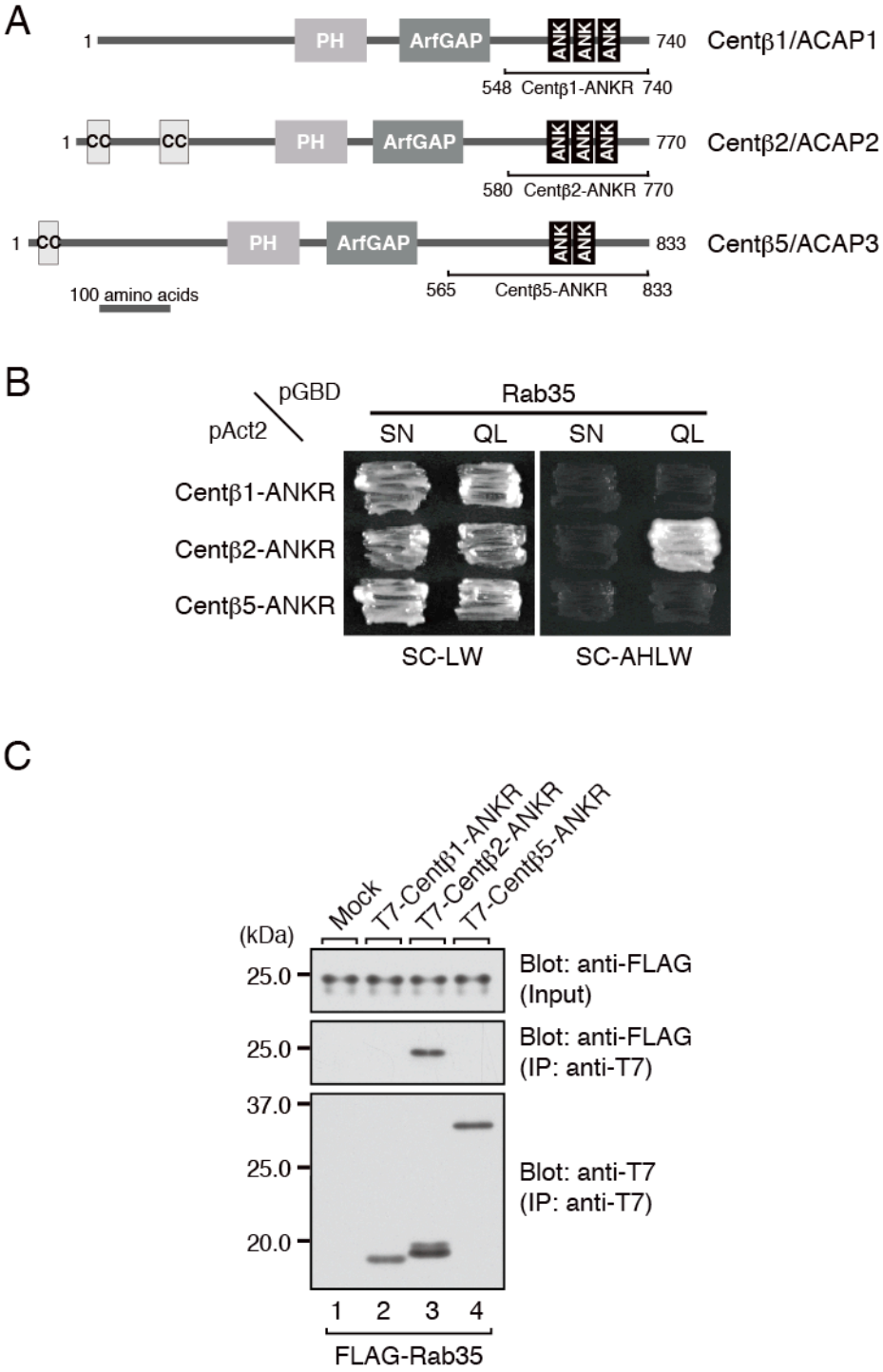

FIGURE 4. Rab35-binding activity of the centaurin-β2 homologues, centaurin-β1 and centaurin-β5.

(A) Schematic representation of the domain organization of centaurin-β1/ACAP1 (Centβ1), centaurin-β2/ACAP2 (Centβ2), and centaurin-β5/ACAP3 (Centβ5).

(B) Centβ2-ANKR, but not Centβ1-ANKR or Centβ5-ANKR, specifically recognized the active form of Rab35. Yeast cells containing pAct2 plasmid expressing

Centβ1-ANKR, Centβ2-ANKR, or Centβ5-ANKR and pGBD plasmid expressing Rab35(QL) (a constitutive active form) or Rab35(SN) (a constitutive negative form) were streaked on SC-LW (left panels) and SC-AHLW (right panels) and incubated at 30°C.

(C) Centβ2-ANKR, but not Centβ1-ANKR or Centβ5-ANKR, interacted with Rab35 in COS-7 cells. Co-immunoprecipitation assays were performed as described in the legend for Figure 1E. The positions of the molecular mass markers (in kilodaltons) are shown on the left.

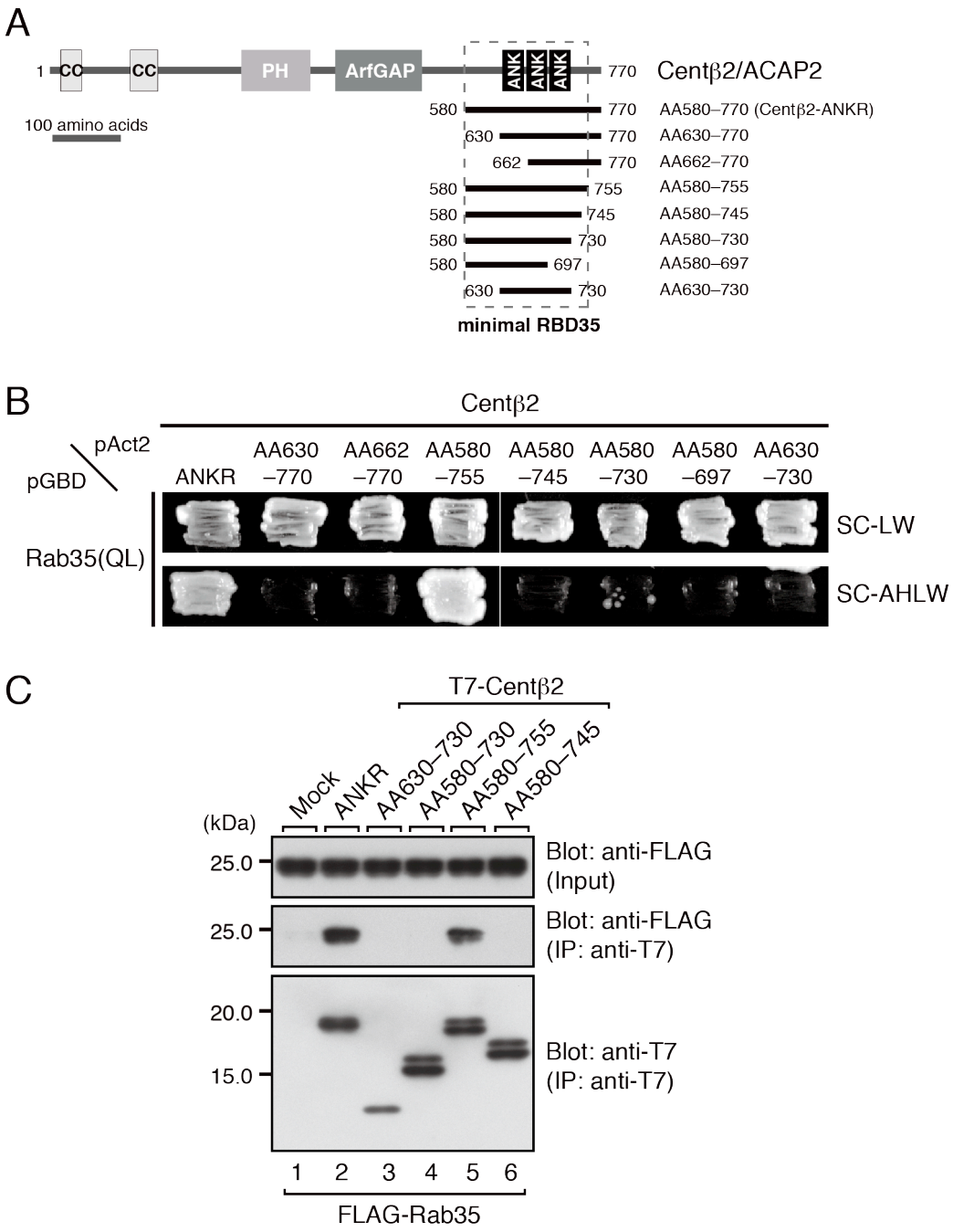

FIGURE 5. Determination of the minimal Rab35-binding site in centaurin-β2. (A) Schematic representation of the deletion mutants of the ANKR domain of centaurin-β2 used in this thesis. Amino acid (AA) numbers are shown on both sides of each construct. The minimal Rab35-binding site (RBD35) determined in this thesis is indicated by enclosure with a broken line.

(B) Rab35 binding activities of the centaurin-β2 deletion mutants. Yeast cells containing pAct2 plasmid expressing Centβ2-ANKR or each Centβ2-ANKR mutant (AA630–770, AA662–770, AA580–755, AA580–745, AA580–730, AA580–697, or AA630–730) and pGBD plasmid expressing Rab35(QL) were streaked on SC-LW (top panel) and SC-AHLW (bottom panel) and incubated at 30°C.

(C) Rab35 binding activity of Centβ2-ANKR mutants (AA630–730, AA580–730, AA580–755, and AA580–745) in COS-7 cells. Co-immunoprecipitation assays were performed as described in the legend for Figure 1E. The positions of the molecular mass markers (in kilodaltons) are shown on the left.

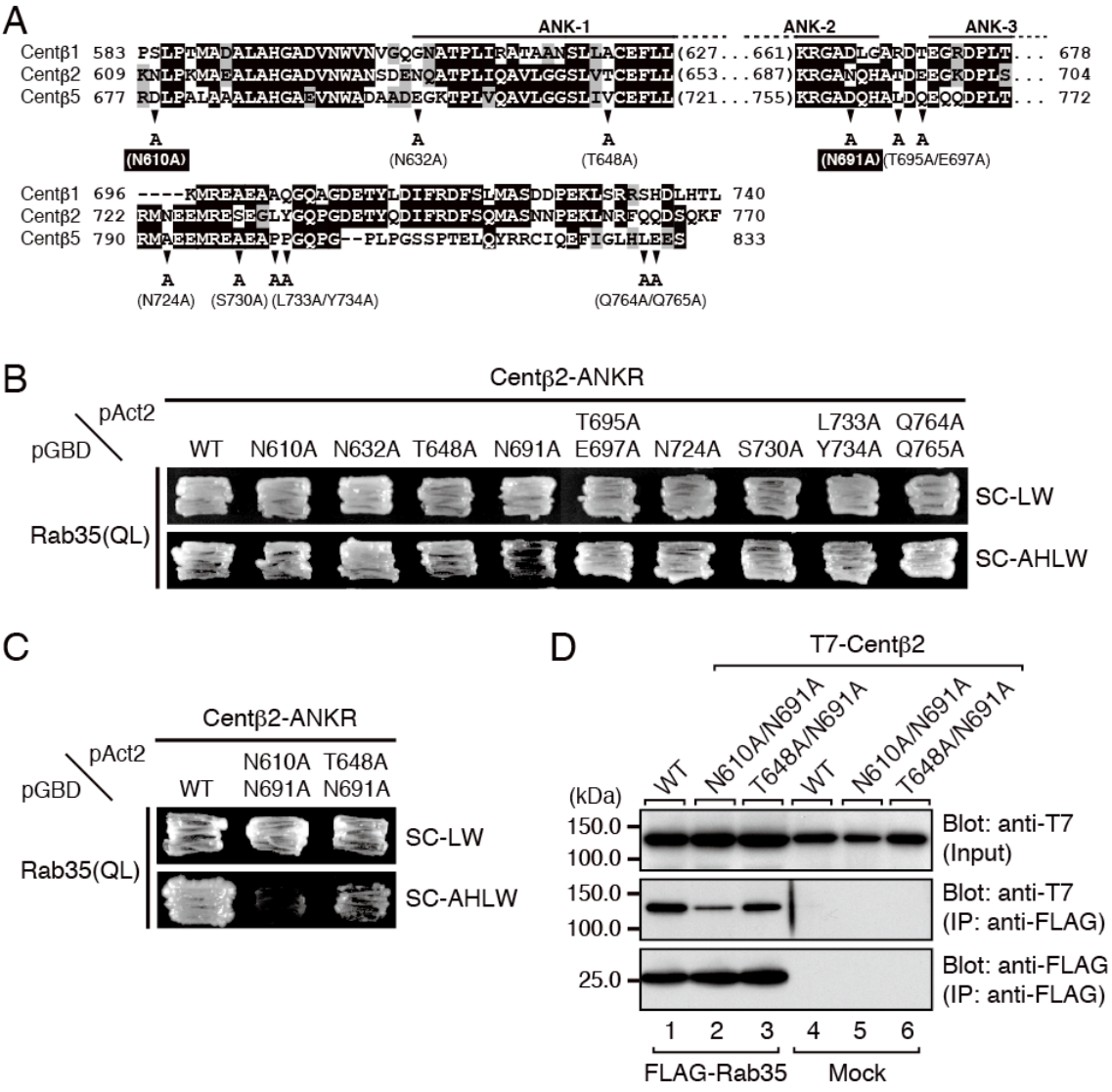

FIGURE 6. Identification of critical residues responsible for the binding of Rab35 in the ANKR domain of centaurin-β2 by site-directed mutagenesis.

(A) Sequence alignment of the ANKR domains of mouse centaurin-β1 (Centβ1), centaurin-β2 (Centβ2), and centaurin-β5 (Centβ5). Amino acid residues in the sequences that are conserved and that are similar are shown against a black background and a shaded background, respectively. The arrowheads indicate the positions of amino acids that are not conserved between Centβ2 and Centβ1 or Centβ5 and were the focus of the Ala-based site-directed mutagenesis.

(B) Rab35 binding activity of Centβ2 as determined by yeast two-hybrid assays. Yeast cells containing pAct2 plasmid expressing Centβ2-ANKR(WT) or each Centβ2-ANKR mutant (N610A, N632A, T648A, N691A, T695A/E697A, N724A,

S730A, L733A/Y734A, or Q764A/Q765A) and pGBD plasmid expressing Rab35(QL) were streaked on SC-LW (top panel) and SC-AHLW (bottom panel) and incubated at 30°C. Based on the growth rate of the yeast cells, the N610A, T648A, or N691A mutation in the Centβ2-ANKR appeared to slightly decrease Rab35 binding activity. (C) Two Asn residues, i.e., Asn-610 and Asn-691, of Centβ2-ANKR are critical for binding Rab35. Yeast two-hybrid assays were performed as described in B.

(D) The N610A/N691A mutation of Centβ2 dramatically decreased Rab35 binding activity, a finding that was consistent with the results of the yeast two-hybrid assays shown in C. Co-immunoprecipitation assays were performed as described in the legend for Figure 1E. The positions of the molecular mass markers (in kilodaltons) are shown on the left.

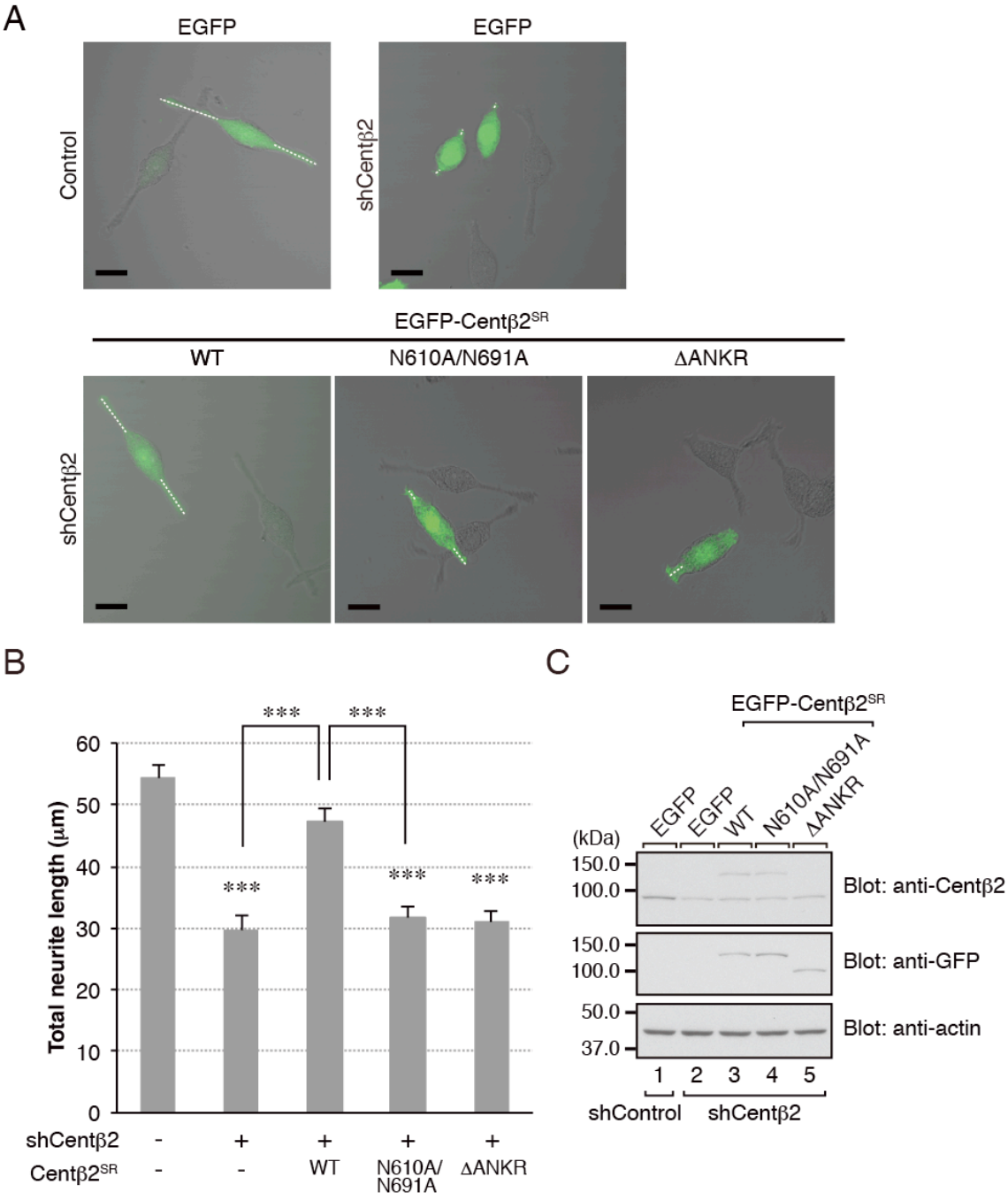

FIGURE 7. Effect of the N610A/N691A mutation of centaurin-β2 on NGF-induced neurite outgrowth of PC12 cells.

(A) Typical images of PC12 cells (merged bright-field images and EGFP fluorescence images) transiently expressing shControl or shcentaurin-β2 (shCentβ2) together with pEGFP-C1 (top row) or pEGFP-C1-Centβ2^{SR}(WT, N610A/N691A, or ΔANKR) (bottom row). The cells were fixed after NGF stimulation for 36 h and examined

under a confocal microscope. Under my experimental conditions, manipulation of centaurin-β2 had no significant effect on the number of neurites (shControl, 2.2 ± 0.05; shCentβ2, 2.0 ± 0.04; shCentβ2 + Centβ2^{SR}(WT), 2.1 ± 0.04; shCentβ2 + Centβ2^{SR}(N610A/N691A), 2.0 ± 0.04; and shCentβ2 + Centβ2^{SR}(ΔANKR), 2.0 ± 0.05 (mean ± SEM)), suggesting that centaurin-β2 is involved in neurite extension rather than in neuritogenesis, the same as Rab35 is. Scale bars, 20 μm.

(B) Quantification of total neurite length shown in A (sum of the lengths of the broken white lines in each PC12 cell). The bars represent the means and SEM of data from three independent experiments (n = 100 cells; more than 30 cells were analyzed in each experiment). **, $p < 0.01$; ***, $p < 0.001$ (one-way ANOVA followed by the Tukey-Kramer test).

(C) Equivalent expression level of EGFP-Centβ2^{SR}(WT, N610A/N691A, or ΔANKR) in shCentβ2-expressing PC12 cells. Cell lysates of PC12 cells expressing shCentβ2 together with EGFP-Centβ2^{SR}(WT, N610A/N691A, or ΔANKR) were subjected to 10% SDS-PAGE followed by immunoblotting with anti-Centβ2 antibody, anti-GFP antibody, and anti-actin antibody. Because our anti-Centβ2 antibody recognized the C-terminal domain of centaurin-β2, it failed to detect EGFP-Centβ2^{SR}(ΔANKR) expression (top panel, lane 5). The positions of the molecular mass markers (in kilodaltons) are shown on the left.

Chapter 2

Rab10 regulates tubular endosome formation through KIF13A/B motors

Abstract

Recycling endosomes are stations that sort endocytic cargoes to their appropriate destinations. Tubular endosomes have been characterized as a recycling endosomal compartment for clathrin-independent cargoes. However, the molecular mechanism by which tubular endosome formation is regulated is poorly understood. In this chapter, I identified Rab10 as a novel protein localized at tubular endosomes by using a comprehensive localization screen of EGFP-tagged Rab small GTPases. Knockout of Rab10 completely abolished tubular endosomal structures in HeLaM cells. We also identified kinesin motors KIF13A/B as novel Rab10-interacting proteins by means of *in silico* screening. The results of this study demonstrated that both the Rab10-binding homology domain and the motor domain of KIF13A are required for Rab10-positive tubular endosome formation. My findings provide insight into the mechanism by which the Rab10–KIF13A/B complex regulates tubular endosome formation.

Introduction

Higher eukaryotic cells contain several functionally distinct endosomal compartments, including an early endosome (EE) and a recycling endosome (RE). Their endosomal compartments sort internalized proteins according to their destinations, e.g., lysosomes, the plasma membrane (PM), and the *trans*-Golgi network (TGN). REs were originally characterized as the interchange to recycle internalized cargoes, such as the transferrin receptor (TfR), from EEs to the PM (1). The endosomal sorting machinery is essential for maintaining the homeostasis that underlies fundamental cellular functions such as intracellular signaling, cell migration, and polarity formation (2, 3).

Recent studies have demonstrated the presence of another distinct RE compartment that is characterized by striking tubular-shaped structures (4, 5). The tubular recycling endosomes, called tubular endosomes, have been shown to be involved in the clathrin-independent endocytic (CIE) pathway and not in the clathrin-mediated endocytic (CME) pathway (6, 7). Tubular endosomes are thought to regulate the sorting and trafficking of CIE cargoes such as CD147 and not CME cargoes such as TfR (8, 9). However, the significance of their tubular structure remains to be determined, in part because of lack of information about the molecular mechanism of tubular endosome formation.

The Rab family of small GTPases are key regulators of membrane traffic that consist of approximately 60 members in mammals. Since each Rab is thought to

regulate different intracellular membrane trafficking pathways, i.e., the secretory pathway, the endocytic pathway, and the recycling pathway, for CME cargoes (10–13), it seems reasonable to expect that a set of Rabs also functions in the formation of tubular endosomes. Actually, several Rab family members, i.e., Rab8A, 11A, 22A, and 35, have been reported to regulate tubular endosome formation (14–17). However, the full repertoire of tubular-endosome-resident Rabs and their roles in tubular endosomes remain to be determined.

In this chapter, I performed a comprehensive localization screening of the Rab subfamily and succeeded in identifying Rab10 as a novel protein predominantly localized at tubular endosomes. Intriguingly, knockout of Rab10 completely disrupted the formation of tubular endosomes. I also identified kinesin motors KIF13A/B as novel Rab10-interacting proteins by means of *in silico* screening and found that their knockout also disrupts tubular endosome formation. My findings suggest that the Rab10–KIF13 complex regulates the formation of tubular endosomes through its motor activity along microtubule tracks.

Materials and Methods

Materials

Anti-Rab22A rabbit polyclonal antibody was raised against GST-Rab22A (18) as an antigen and purified as described previously (19). The following commercially available antibodies were used in this study: anti-human Lamp1 (clone H4A3, sc-20011) and anti-c-Myc (9E10, sc-40) mouse monoclonal antibodies from Santa Cruz Biotechnology (Dallas, TX); HRP-conjugated FLAG tag mouse monoclonal antibodies (M2, A8592) from Sigma-Aldrich (St. Louis, MO); anti-β-actin mouse monoclonal antibody (G043) from Applied Biological Materials (Richmond, BC, Canada); anti-Rab8 (610845; reacting with both Rab8A and Rab8B) and anti-GM130 mouse monoclonal antibodies (35/GM130, 610822) from BD Biosciences (San Jose, CA); anti-Rab10 (clone D36C4, 8127), anti-Rab8 rabbit (clone D22D8, 6975; for immunofluorescence), and anti-EEA1 rabbit monoclonal antibodies (clone C45B10, 3288) from Cell Signaling Technology (Danvers, MA); anti-Rtn4/NogoA rabbit monoclonal antibody (AHP1799) from Bio-Rad (Hercules, CA); anti-LBPA mouse monoclonal antibody (clone 6C4, Z-PLBPA) from Echelon Biosciences (Salt Lake City, UT); anti-LC3 (PM036) and anti-GFP (598) rabbit polyclonal antibodies from MBL (Woburn, MA); mouse anti-MICAL-L1 (H00085377-B01P) from Abnova (Taipei, Taiwan); anti-KIF13A (A301-077A) rabbit polyclonal antibody from Bethyl Laboratories (Montgomery, TX); anti-CD147 mouse monoclonal antibody (clone HIM6, 306202) from Biolegend (San Diego, CA); anti-KIF13B rabbit polyclonal antibody

(NBP1-83398) and anti-Rab22B/31 mouse monoclonal antibody (1C6, H00011031-M01) from Novus Biologicals (Littleton, CO) ; anti-RFP rabbit polyclonal antibody (600-401-379) from Rockland (Gilbertsville, PA) ; anti-TGN46 rabbit polyclonal antibody (ab50595) from Abcam (Cambridge, MA) ; anti-HA rat polyclonal antibody (3F10, 11867423001) from Roche Diagnostics (Indianapolis, IN); anti-TfR mouse monoclonal antibody (clone H68.4, 13-6800), and Alexa Fluor–labeled secondary antibodies from Thermo Fisher Scientific (Waltham, MA).

Plasmid Construction

The pMRX-IRES-puro retroviral vector was a kind gift from Shoji Yamaoka (20). cDNAs encoding the mouse Rabs (1A, 2A, 3A, 4A, 5A, 6A, 7, 7B/42, 8A, 9A, 10, 11A, 12, 13, 14, 15, 17, 18, 19, 20, 21, 22A, 23, 24, 25, 26, 27A, 28, 29, 30, 32, 33A, 34, 35, 36, 37, 38, 39A, 40C, 42/43, and 43/41) (21) were subcloned into the pMRX-puro-EGFP vector. cDNAs encoding Rab10, Rab8A, and Rab22A were subcloned into the pMRX-bsr vector or the pMRX-bsr-Myc vector. cDNA encoding EMTB (AA153-419 of human MAP7, transcript variant 4) was amplified from Marathon-Ready human testis cDNA (Clontech-Takara Bio, Shiga, Japan) by PCR with the following pair of oligonucleotides: 5’-GTCCGGACTCGGATCCGCAGTGCGAAGCGAAACAG-3’ (forward primer; homologous sequence with the 3’ end of the linearized vector underlined) and 5’-ATTTACGTAGCGGCCCTAAGAGCCCTCAGGTGGTGTT-3’ (reverse primer; homologous sequence with the 5’ end of the linearized vector underlined), and

subcloned into the pMRX-puro-EGFP vector and pMRX-bsr-mStr vector with an In-Fusion HD cloning kit (Clontech-Takara Bio). cDNA encoding LifeAct-mCherry (kindly provided by Dr. Kazumasa Ohashi, Tohoku University) was subcloned into the pMRX-bsr vector. cDNAs encoding the tail domains of mouse KIF13A and KIF13B were prepared as described previously (22). cDNAs encoding the motor domains of mouse KIF13A and KIF13B were amplified from Marathon-Ready mouse brain and testis cDNAs (Clontech-Takara Bio) by PCR with the following pairs of oligonucleotides: 5'-GGATCCATGTCGGATACGAAGGTAAA-3' (Kif13A motor forward primer; *Bam*HI site underlined) and 5'-CCGCGGAACTGGTTTCTCTCTCAA-3' (Kif13A motor reverse primer); 5'-AGATCTATGGGAGACTCCAAAGTGAA-3' (Kif13B motor forward primer; *Bgl*II site underlined) and 5'-CAGATCTCGGATAATCCGAG-3' (Kif13B motor reverse primer). cDNAs encoding the full length of mouse KIF13A and KIF13B were prepared by combining their motor domain and tail domain constructs, and subcloned into the pMRX-puro HA vector or pMRX-bsr Myc vector. cDNAs encoding mouse KIF13A/B (ΔRHD10) mutants were prepared by inverse PCR using a KIF13A/B-harboring vector as a template and the following pairs of oligonucleotides: 5'-CCGATGCAGTGCTGGTGCCCGCCCCTGGCAGCG-3' (KIF13A ΔRHD10 forward primer) and 5'-CCAGCACTGCATCGGACCATCTCTCTCTTACA-3' (KIF13A ΔRHD10 reverse primer); 5'-TCAATGCAGTGATGGTGCCTTCTGCTGGGAGTG-3' (KIF13B ΔRHD10 forward primer) and 5'-CCATCACTGCATTGAGCCATTTTCTACGAAGC-3'

(KIF13B ΔRHD10 reverse primer). pGEX-6P-1-GFP-nanobody (23) was kindly provided by Dr. Kazuhisa Nakayama (Kyoto University).

Cell Culture, Transfection, Infection, and Drug Treatment

HeLaM cells, COS-7 cells, and Plat-E cells (a kind gift from Dr. Toshio Kitamura, The University of Tokyo) were grown at 37°C in Dulbecco's modified Eagle medium (D-MEM) (044-29765; FUJIFILM Wako Pure Chemical, Osaka, Japan) supplemented with 10% fetal bovine serum (FBS), 100 U/ml penicillin G, and 100 μg/ml streptomycin in a 5% CO_2 incubator. For live-cell imaging, D-MEM with HEPES (044-32955; FUJIFILM Wako Pure Chemical) was used instead of D-MEM with phenol red. Transfection of plasmids into HeLaM cells and Plat-E cells was performed by using Lipofectamine 2000 (Invitrogen) according to the manufacturer's protocol. To establish stable cell lines, retrovirus production in Plat-E cells and retrovirus infection were performed as described previously (24). Plasmid mixtures containing pMRX vector and pLP/VSVG (Thermo Fisher Scientific, MA) were transfected into Plat-E cells, and the culture medium containing the desired retroviruses was collected. HeLaM cells were infected by using the retrovirus-containing medium and 5 μg/ml polybrene. Stable cell lines were selected by using puromycin (2 μg/ml for 48 h, Merck Millipore, MA) and blasticidin S (5 μg/ml for 24 h, FUJIFILM Wako Pure Chemical). Cells were exposed for 1 h to 10 μM cytochalasin D or 10 μg/ml nocodazole under the above culture conditions.

CRISPR/Cas9 Gene KO

Rab8A/B-, Rab10-, Rab22A/B-, KIF13A-, KIF13B-, and KIF13A/B-KO HeLaM cell lines were established by means of the following procedures. pSpCas9(BB)-2A-Puro vector (Addgene; #48139) was used to generate a single guide RNA (sgRNA). The following sgRNA sequences were designed by using the CRISPRdirect website (http://crispr.dbcls.jp/): sgRNA sequences targeting human Rab8A (sense, 5'-CACCGATTAGGACCATAGAGCTCGA-3' and antisense, 5'-AAACTCGAGCTCTATGGTCCTAATC-3'); human Rab8B (sense, 5'-CACCGCTCCTGCTGATCGGCGACTC-3' and antisense, 5'-AAACGAGTCGCCGATCAGCAGGAGC-3'); human Rab10 (sense, 5'-CACCGGATCGGGGATTCCGGAGTGG-3' and antisense, 5'-AAACCCACTCCGGAATCCCCGATCC-3'); human Rab22A (sense, 5'-CACCGTTAGCACCAATGTACTATCG-3' and antisense, 5'-AAACCGATAGTACATTGGTGCTAAC-3'); human Rab22B (sense, 5'-CACCGCATCGTGTGTCGATTTGTCC-3' and antisense, 5'-AAACGGACAAATCGACACACGATGC-3'); human KIF13A (sense, 5'-CACCGGATATGCAGACCGAGCCAAA-3' and antisense, 5'-AAACTTTGGCTCGGTCTGCATATCC-3'); and human KIF13B (sense, 5'-CACCGAGTGAACGAGCAACGAAGAC-3' and antisense, 5'-AAACGTCTTCGTTGCTCGTTCACTC-3'). The sgRNA expression constructs were transfected into HeLaM cells, and 24 h later 2 μg/ml puromycin (Merck Millipore) was added to the culture medium to select transfected cells. Puromycin was removed

after an additional 48 h, and the cells were cloned by limited dilution. Clonal lines were isolated and analyzed by immunoblotting with a specific antibody to check for absence of expression of target proteins.

Purification of GST Fusion Proteins

GST-tagged GFP nanobody was expressed in *Escherichia coli* JM109 and purified as described previously (25).

Immunoblot Analysis

HeLaM cells were lysed in an SDS sample buffer (62.5 mM Tris-HCl, pH 6.8, 2% 2-mercaptoethanol, 10% glycerol, and 0.02% bromophenol blue) and boiled. The samples were subjected to SDS-PAGE and then transferred to polyvinylidene difluoride membranes (Merck Millipore). The membranes were blocked with PBS-T (0.1% Tween 20 in PBS) containing 1% skim milk and incubated for 1 h with specific primary antibodies. The membranes were subsequently incubated for 1 h with appropriate HRP-conjugated secondary antibodies, and immunoreactive bands were detected by using enhanced chemiluminescence and X-ray films or the ChemiDoc Touch imaging system (Bio-Rad).

Co-immunoprecipitation Assays

COS-7 cells co-expressing mStr-Rab10 and EGFP or EGFP-tagged KIF13(A or B)-tail were lysed in a lysis buffer (50 mM HEPES-KOH, pH 7.2, 150 mM NaCl, 10

mM $MgCl_2$, 1% Triton X-100, and protease inhibitor cocktail; Roche, Basel, Switzerland). The lysates were centrifuged at 17,400 × *g* for 10 min at 4°C, and the supernatants were incubated for 1 h at 4°C with 5 μl of glutathione-Sepharose 4B beads (wet volume) (GE Healthcare, Little Chalfont, UK) and 1μg of GST-tagged GFP nanobody. The beads were washed with a washing buffer (50 mM HEPES-KOH, pH 7.2, 150 mM NaCl, 10 mM $MgCl_2$, and 0.1% Triton X-100) three times and boiled in the SDS sample buffer. The samples then were subjected to SDS-PAGE and analyzed by immunoblotting with appropriate antibodies.

Immunofluorescence Microscopy

For the immunofluorescence analysis, cells were cultured on coverslips, fixed with 4% paraformaldehyde in PBS for 10 min, and permeabilized for 10 min with 0.05% saponin in PBS containing 0.1% gelatin. The coverslips were incubated for 1 h with primary antibodies and subsequently incubated for 1 h with appropriate Alexa Fluor-conjugated secondary antibodies. The samples were mounted using ProLong Gold Antifade Mountant (Thermo Fisher Scientific). The stained cells were captured with an FV1000D confocal fluorescence microscope through a 60× oil/1.4 NA Plan Apochromatic objective lens and Fluoview software (Olympus, Tokyo, Japan). Super-resolution images were acquired by using the OSR system (Olympus) of an FV1000D confocal fluorescence microscope.

Live-cell imaging

Live-cell imaging was performed with an Andor Dragonfly spinning disk scanning unit (Dragonfly200) or a Zeiss Yokogawa spinning disk scanning unit (CSU-W1) coupled with an inverted Olympus IX83 microscope equipped with a 60× oil/1.35 NA Plan Apochromatic objective lens. During live-cell imaging, the culture dish was mounted in a chamber (STRG-WELSX-SET; Tokai Hit, Shizuoka, Japan, or STXG-IX3WX-SET; Tokai Hit) to maintain the cells at 37°C and under a 5% CO_2 atmosphere.

Quantification of Tubular Endosomes

The number of cells containing at least one tubule >20 μm in length was manually measured. The number of cells containing at least one tubule >20 μm in length was counted in each experiment (more than 20 cells were analyzed in each experiment). Total tubule length (i.e., sum of the length of all tubules) per cell was measured by using Fiji (https://fiji.sc) and the population profile was created (Figure 4H). Maximum intensity z-projected images were binarized and then skeletonized by LpxLineExtract, which is invoked by Lpx_Filter2d plug-ins (filter = lineFilters, linemode = lineExtract) in the LPixel ImageJ plugins package (https://lpixel.net/services/research/lpixel-imagej-plugins/) (26). The >5 μm skeletonized lines in the images were extracted by using the analyze particles function in Fiji. Total tubule length in each cell was measured by using the measure function in Fiji, and a histogram analysis of the data was performed by using the Excel software program (Microsoft, Redmond, WA).

Colocalization Analysis

The PCC values were calculated for more than 4 maximum intensity z-projected images from each experiment by using Coloc 2, a Fiji plugin for colocalization analysis (http://imagej.net/Coloc_2). The line plot profile of the yellow arrows in Figures 1E and 5A was obtained by using the plot profile function in Fiji.

Bioinformatics Analysis

The RHD10 of KIF13A/B was identified by using the RBD10 of MICAL1 (isoform 3 of human: AA939-1080) or EHBP1 (isoform 1 of human: AA1070-1212) as a search query in PSI-BLAST searches, followed by a DELTA-BLAST search. The 3D-homology modeling of the RHD10 of KIF13A was performed by using the Modeller9.19 software (27), incorporated in the UCSF Chimera interactive graphic interface (28). Rab10–MICAL1 complex (PDB: 5LPN) was used as a template.

Statistical Analysis

All quantitative data are expressed as the means and SEM. Tukey's test, Dunnett's test, unpaired Student's *t* test, and Pearson's χ^2 test were performed to evaluate the statistical significance of differences between samples. *P* values <0.05 were regarded as statistically significant.

Results

Comprehensive Localization Screening for EGFP-Rabs Identified Rab8 and Rab10 as Specific Markers for Tubular Endosomes

To prepare a list of Rabs that specifically localize at tubular endosomes, I established a library of HeLaM cells that stably express EGFP-tagged Rab subfamily members (Rab1A–43) and performed a localization screening. First, I defined a tubular endosome as a tubular structure >20 μm in length and manually counted the number of cells containing at least one EGFP-positive tubular endosome (Figure 1A and 1B, blue bars). Second, I immunostained HeLaM cells with antibody against MICAL-L1, a well-known tubular endosome marker (14) and then calculated Pearson's correlation coefficient (PCC) values for the relation between EGFP-Rabs and MICAL-L1 (Figure 1A and 1B, orange bars). The results showed that 10 of the Rab subfamily members tested, i.e., Rab5A, 8A, 10, 11A, 13, 17, 21, 22A, 23, and 35, were localized at tubular endosomes, but that neither EGFP alone nor EGFP-Rab1A was associated with tubular endosomes (Figure 1B, blue bars, and Figure 2). It should be noted that tubules positive for 8 Rabs (Rab8A, 10, 11A, 13, 17, 22A, and 35) were colocalized with MICAL-L1, but that Rab5A-positive tubules and Rab21-positive tubules were not (Figure 2), suggesting the presence of subdomains in the tubular endosomes. Because these tubular-endosome-resident Rabs are known to localize at REs, EEs, and/or the PM (29–38), tubular endosomes are likely to be part of recycling pathways, as described previously (5). Consistent with previous reports (8, 15, 16),

tubular localization of Rab8A/11A/22A was also observed, thereby validating the results of my screenings. Two of the tubular-endosome-resident Rabs I identified, Rab8 and Rab10 showed higher values with respect to the percentage of cells with Rab-positive tubular endosomes (more than 80%) and to the PCC value for the relation between EGFP-Rabs and MICAL-L1 (more than 0.4) (Figure 1B), and I therefore decided to focus on them for further analysis.

Because Rab10 had previously been shown to be localized at REs, the TGN, or endoplasmic reticulum (ER) in other cell types (31, 39, 40), I investigated the subcellular localization of endogenous Rab8 and Rab10 in HeLaM cells. The same as EGFP-Rab8 and -Rab10, I found that endogenous Rab8 and Rab10 were well colocalized with MICAL-L1 at tubular endosomes (Figures 1C–D and 2). I also compared the localization of EGFP-Rab10 with several organelle markers to determine its subcellular localization. The results showed that EGFP-Rab10 was significantly colocalized with MICAL-L1 (PCC = 0.51 ± 0.04) as compared with TGN46 (a TGN marker; PCC = 0.32 ± 0.03), GM130 (a *cis*-Golgi marker; PCC = 0.26 ± 0.04), TfR (an RE marker; PCC = 0.04 ± 0.03), EEA1 (an EE marker; PCC = 0.13 ± 0.04), LC3 (an autophagosome marker; PCC = 0.05 ± 0.05), LAMP1 (a lysosome marker; PCC = 0.04 ± 0.01), LBPA (a late endosome [LE] marker; PCC = 0.04 ± 0.03), or RTN4 (an ER marker; PCC = -0.03 ± 0.04) (Figure 3A and 3B), confirming that Rab10 mainly marks tubular endosomes rather than conventional TfR-positive REs in HeLaM cells. Although Rab10 was partially colocalized with TGN46, brefeldin A treatment, which disrupts the Golgi complex, did not affect the EGFP-Rab10-positive tubules (Figure 3C

and 3E), but it resulted in a decrease in the PCC for the relation between EGFP-Rab10 and TGN (PCC = 0.04 ± 0.03) (Figure 3D). These results suggest that EGFP-Rab10-positive tubules are distinct from the tubular carriers in the TGN, which is a part of the pathway for newly synthesized proteins (41). The discrepancy between the Rab10-localization results obtained in this study (HeLaM cells) and previous studies (other cell types) may be explained by Rab10 localization being cell- or tissue-specific.

To determine whether Rab10-positive tubules preferentially transport CIE cargoes rather than CME cargoes, I compared EGFP-Rab10 localization with the localization of Tf and CD147, which are internalized into the RE via the CME pathway and the CIE pathway, respectively. To do so, I observed HeLaM cells stably expressing EGFP-Rab10 that had internalized both Alexa594-Tf and anti-CD147 antibody. The results showed that EGFP-Rab10 clearly colocalized with the internalized CD147 at tubular endosomes and did not colocalize with the internalized Tf (Figure 1E and 1F). These results are consistent with previous reports that tubular endosomes contain CIE cargoes, not CME cargoes.

Rab10 Is Required for Tubular Endosome Formation and its Dynamics Depends on Microtubules

To determine whether Rab8 and Rab10 are required for tubular endosome formation and reveal their relationships, I generated Rab8A/B-double knockout (Rab8-DKO) and Rab10-knockout (Rab10-KO) cell lines by using the CRISPR/Cas9 system (Figure 4A and 4B) and examined the Rab8-DKO cells for the presence of

EGFP-Rab10-positive tubules and the Rab10-KO cells for the presence of EGFP-Rab8-positive tubules. EGFP-Rab10-positive tubules were still observed in the Rab8-DKO cells, and their overall localization was unaltered even in the Rab8-DKO cells stably re-expressing Myc-Rab8A (Figure 4C and 4E). These results were consistent with the previous finding that Rab8 itself is dispensable for tubular endosome formation (14, 42). By contrast, Rab10 KO resulted in complete dispersion of both the Rab8- and MICAL-L1-positive tubules (Figure 4D, top panels, and Figure 5A), and re-expression of Rab10 in Rab10-KO cells clearly rescued this phenotype (Figure 4D, bottom panels, 4F, and 4G). On the other hand, Rab10 KO had no effect on the level of Rab8 expression or MICAL-L1 expression (Figure 4B), indicating that Rab10 KO causes disruption of both tubules without affecting the levels of expression of tubular components. To quantitatively evaluate the difference between Rab10-KO cells and Rab10-KO cells stably re-expressing Rab10, I measured the total length of MICAL-L1-positive tubules in each cell. The results showed a significant difference between the population profile of total tubule length of Rab10-KO cells and Rab10-KO cells stably re-expressing cells (Figure 4H). Intriguingly, other tubular-endosome-resident Rabs, i.e., EGFP-Rab5A, -Rab11A, -Rab13, and -Rab22A (Figure 1B and 1C), as well as Rab8A were not localized at the tubular endosomes in Rab10-KO cells (Figure 5A), suggesting that Rab10 is an essential constituent of tubular endosomes. To determine the hierarchical relationship between Rab10 and Rab22A, a regulator of tubular endosomes (16), I generated a Rab22A/B-double knockout (Rab22-DKO) cell line (Figure 5B) and examined the effects of Rab22A/B

depletion on EGFP-Rab10 localization. The results showed that Rab22A/B are required for the formation of EGFP-Rab10-positive tubules (Figure 5C and 5D), although Rab10 is also necessary for the formation of EGFP-Rab22A-positive tubules (Figure 5A). These results indicate that Rab10 and Rab22A/B cooperatively regulate tubular endosome formation.

To evaluate tubular endosome dynamics, I performed live-cell time-lapse imaging of HeLaM cells stably expressing EGFP-Rab10. Examination of the images revealed that EGFP-Rab10-positive tubules are highly dynamic structures that frequently extend, branch, and retract (Figure 6A). Previous studies have shown that actin filaments, not microtubules, are required for Rab10-binding protein EHBP1-positive tubules in the intestinal epithelium of *C. elegans* (43), whereas microtubules, not actin filaments, are required for the formation of Rab11A- and Rab22A-positive tubules in HeLa cells (5, 15). To determine whether the formation of Rab10-positive tubules in HeLaM cells depends on actin filaments or microtubules, I treated the cells with cytochalasin D and nocodazole, which are inhibitors of actin polymerization and microtubule polymerization, respectively. Cytochalasin D treatment disrupted actin filaments, but dynamic tubular endosomes were still observed (Figure 6B and 6C), whereas nocodazole treatment dispersed the EGFP-Rab10-positive tubules into the cytoplasm (Figure 6A and 6B). Consistent with these results, EGFP-Rab10-positive tubules were well colocalized with mStr (monomeric Strawberry)-EMTB (Figure 6D, arrowheads), which is an ensconsin microtubule-binding domain that can be used as a microtubule probe (44). Moreover, EGFP-EMTB localization in Rab10-KO cells seemed unaltered

in comparison with its localization in parental cells or Rab10-KO cells stably re-expressing Rab10 (data not shown), indicating that the disruption of tubular endosomes in Rab10-KO cells is not caused by microtubule depolymerization. These results taken together indicate that tubular endosomes are formed in a microtubule-dependent manner.

KIF13A/B are Novel Rab10-interacting Proteins

Since Rab proteins are generally thought to regulate membrane trafficking through the functions of their effectors, I focused my attention on the effectors of Rab10 as a means of gaining insight into the molecular mechanism by which Rab10 regulates tubular endosome formation (11). Because microtubules are required for tubular endosome formation (Figure 6B and 6C), I hypothesized that microtubule-associated Rab10 effectors are involved in the process. I initially investigated previously reported Rab10 effectors, including proteins containing a bivalent MICAL/EHBP Rab binding domain (MICAL1, MICAL3, MICAL-cl, MICAL-L1, MICAL-L2, EHBP1, EHBP1L1, and C16orf45) (45), myosin-Va/b (39, 46), JIP1 (47), Sec16A (48), Evi5 (49), and Lgl1 (50), but I was unable to identify any good candidates, because siRNA-mediated knockdown of these Rab10 effectors had no effect on the formation of EGFP-Rab10-positive tubules (data not shown).

To identify a novel Rab10 effector(s) that associates with microtubules, I performed *in silico* screening. I performed DELTA-BLAST searches by using the known Rab10-binding domain (RBD10) of MICAL1 or EHBP1 (45) as bait, followed

by PSI-BLAST, and then selected microtubule-associated proteins among the candidate Rab10 effectors. By so doing I succeeded in obtaining a list of proteins containing an RBD10 homology domain, named RHD10, and identified the molecular motors KIF13A/B as candidates for novel Rab10 effectors that interact with microtubules (Figure 7A).

KIF13A/B belong to the kinesin-3 family, which is evolutionarily conserved in higher eukaryotes and whose members function as organelle transporters in the dimer state (51, 52). The sequential BLAST search showed that the amino acid (AA) sequence AA1102–1146 of KIF13A and AA sequence AA1099–1143 of KIF13B are similar to both RBD10s of MICAL1 and EHBP1 (Figure 7A, orange lines, and 7B). To structurally compare the RHD10 of KIF13A and RBD10 of MICAL1, I performed 3D-homology modeling of the RHD10 based on the crystal structure of the Rab10–MICAL1 complex (PDB: 5LPN) by using MODELLER software (27). As expected, the RHD10 of KIF13A overlapped the Rab10-binding region of the RBD10 of MICAL1 (Figure 7C). To confirm the interaction between Rab10 and KIF13A, I transiently co-expressed EGFP-KIF13A/B-tail, which contain the RHD10 (Figure 7D), and mStr-Rab10 in COS-7 cells and evaluated their interaction by immunoprecipitation using glutathione-Sepharose beads coupled with a GST-fused GFP nanobody. The results showed that EGFP-KIF13A/B, not EGFP alone, interacted with mStr-Rab10 (Figure 7E, top panel), indicating that KIF13A/B are novel Rab10-interacting proteins.

Next, I investigated the subcellular localization of Myc-KIF13A in HeLaM cells. Consistent with the results of the co-immunoprecipitation assays (Figure 7E),

Myc-KIF13A was well colocalized with EGFP-Rab10 at tubular endosomes (Figure 8A and 8B). By contrast, a KIF13A(ΔRHD10) mutant that lacks an RHD10 (Figure 8C), had lost the ability to localize at Rab10-positive tubules (Figure 8A, 8B, and 8D). Similarly, EGFP-KIF13B-tail(WT), but not the ΔRHD10 mutant, was colocalized with mStr-Rab10 at tubular endosomes (Figure 9A and 9B). To determine whether the tubular endosome localization of KIF13A depends on Rab10, I investigated its localization in Rab10-KO cells. As expected, the same as the KIF13A(ΔRHD10) mutant in the parental cells, the Myc-KIF13A in the Rab10-KO cells did not localize at any tubular structures at all (Figure 8E and 8F), although Rab10-KO itself did not affect the level of KIF13A/B expression (Figure 8G). These results suggest that KIF13A/B are localized at tubular endosomes through their Rab10-interaction.

Both the Rab10-binding Homology Domain and the Motor Domain of KIF13A Are Required for Tubular Endosome Formation

Previous studies have shown that certain kinesin motors together with microtubules contribute to organelle tubulation through their motor activity along microtubule tracks (53, 54). I therefore hypothesized that KIF13A/B regulate the tubulation of Rab10-resident endosomes through their motor activity. To test this hypothesis, I established KIF13A-KO, KIF13B-KO, and KIF13A/B-DKO cell lines (Figure 10A) and examined the tubular endosomes in these cells. The results showed that neither KIF13A-KO cells nor KIF13A/B-DKO cells contained MICAL-L1-positive tubules (Figure 10B and 10C), the same as Rab10-KO cells, which also lacked

MICAL-L1-positive tubules (Figure 4D). There were also fewer MICAL-L1-positive tubules in the KIF13B-KO cells, but the phenotype was much less severe than that of the KIF13A-KO cells (Figure 10C), indicating that KIF13A plays the predominant role in tubular endosome formation. To further investigate the functional redundancy of KIF13A/B, I evaluated the effect of KIF13B overexpression on tubular endosomes in KIF13A-KO cells. The results showed that KIF13B overexpression in KIF13A-KO cells rescued the dispersion of tubular endosomes, the same as KIF13A overexpression had (Figure 11), suggesting that KIF13A/B have redundant functions in tubular endosome formation. The level of KIF13B expression in HeLaM cells may be much lower than that of KIF13A, or KIF13A may have greater ability to facilitate tubule formation than KIF13B does, even if their expression level in HeLaM cells is similar.

To further define the importance of the RHD10 and motor activity of KIF13A in tubular endosome formation, I re-expressed KIF13A mutants (ΔRHD10 and tail, which lacks an N-terminal motor domain; see also Figures 7D and 8C, respectively) in KIF13A-KO cells. EGFP-Rab10 was not localized at tubular endosomes in KIF13A-KO cells, and re-expression of KIF13A(WT) clearly rescued this phenotype (Figure 10D and 10F). By contrast, re-expression of neither KIF13A mutant (tail or ΔRHD10) restored EGFP-Rab10-positive tubular endosomes (Figure 10D and 10F), even though equivalent amounts of proteins were expressed under my experimental conditions (Figure 10E). I therefore concluded that both the RHD10 and the motor domain of KIF13A are required for tubular endosome formation in HeLaM cells.

Discussion

In the present thesis, I performed a comprehensive localization screening for Rabs that are localized on tubular endosomes and succeeded in identifying 10 Rabs, including 6 novel ones. One of them, Rab10, and its interactor KIF13A/B motors were found to be essential factors for the formation of tubular endosomes in HeLaM cells. Because Rab10-positive tubular endosomes are sensitive to nocodazole (Figure 6B) and likely depend on KIF13A/B motor activity (Figure 10), I propose the following model for tubular endosome formation (Figure 12A): Rab10 recruits KIF13A/B to recycling (or early) endosomes, and the Rab10–KIF13 complex together with microtubules facilitates tubulation through KIF13 motor activity. Although several kinesin-3 family members (e.g., KIF1) are known to interact with organelles through their lipid-binding domains, e.g., a pleckstrin homology (PH) domain (52), KIF13A/B lack such a domain. Thus, Rab10 is likely to function as a molecular scaffold for the recruitment of KIF13A/B to tubular endosomes. Moreover, the motor activity of KIF13A has been shown to mediate vesicle tubulation *in vitro* (54), a finding that supports the validity of my model.

How do the Rabs that localize at tubular endosomes contribute to their formation or functions? Based on the results of previous studies on the functions of tubular endosomal Rabs taken together with my own findings in the present study, I propose a model that would explain how these Rabs coordinate tubular endosome formation (Figure 12B). Since tubular endosome formation has previously been shown to be

involved in the Arf6-dependent endocytic pathway for CIE cargoes (55, 56), it seems reasonable to expect the origin and the fate of tubular endosomes or CIE cargoes to be as follows: formation of CIE-cargo-carrying vesicles from the PM (Step 1); vesicle-to-tubular endosome transition (Step 2); CIE cargo sorting/transport to the PM, other RE compartments (e.g., Tf-positive RE), or the TGN (Step 3) (Figure 12B).

My Rab localization screen identified novel MICAL-L1-positive tubular-endosome-resident Rabs (Rab10, 13, 17, and 23) in addition to the known Rabs (Rab8A, 11A, 22A, and 35). Rab13 and Rab35 are likely to participate in Step 1, because they are mainly localized at the PM (57, 58) and regulate certain types of Arf6-dependent endocytosis (59, 60). In Step 2, EE-resident Rab22A, in addition to Rab10, is indispensable for tubular endosome formation (Figure 5D). In Step 3, membrane scission must occur before CIE cargo sorting/transport to other organelles (Figure 6A). I think that Rab8 is the most likely candidate for the regulator in this process, because it is known to form a complex with EHBP1L1–Bin1–dynamin and regulates membrane scission (42). Rab11 and Rab17 may also be involved in Step 3 (or Step 2), because they are mainly localized at Tf-positive REs and regulate its trafficking (32, 61). It should be noted that Rab11 also interacts with KIF13A through the C-terminal region, which does not contain the RHD10 region (62), although Rab11 itself is not necessary for tubular endosome formation (15, 16). I therefore speculate that KIF13A initially interacts with Rab10 in the process of tubular endosome formation and then interacts with Rab11A in the process of CIE cargo sorting/transport from tubular endosomes. Further studies will be necessary to fully understand the functional relationships or

hierarchy of tubular-endosome-resident Rabs in tubular endosome formation and function.

What is the physiological role of Rab10-positive tubular endosomes? There are two tasks that must be accomplished to answer this question: one task is compiling the entire list of tubular endosome cargoes and the other task consists of identifying specific cells that contain tubular endosomes *in vivo*. A certain acidic amino acid cluster of CIE cargoes has already been shown to be a sufficient sorting signal for tubular endosome localization (5, 63), and, intriguingly, forward genetic screening by the gene-trap method has identified Rab10 as a candidate involved in the trafficking of the acidic-cluster-containing proteins (64). Thus, it is plausible to consider the acidic-cluster-containing proteins good candidates for the cargoes of Rab10-positive tubular endosomes. On the other hand, the *in vivo* role of Rab10-positive tubular endosomes is poorly understood, because Rab10-KO mice exhibit embryonic lethality (65) and specific cells or tissues containing tubular endosomes have not been identified. Thus, a future detailed analysis of *in vivo* Rab10 distribution/localization and Rab10 conditional KO mice in various cells or tissues (66, 67) is needed. Identification of acidic-cluster-containing CIE cargoes and specific cells containing Rab10-positive tubular endosomes will be necessary to elucidate the physiological significance of the formation and function of tubular endosomes.

References

1. Maxfield, F. R., and McGraw, T. E. (2004) Endocytic recycling. *Nat. Rev. Mol. Cell Biol.* **5**, 121–132

2. Doherty, G. J., and McMahon, H. T. (2009) Mechanisms of endocytosis. *Annu. Rev. Biochem.* **78**, 857–902

3. Scita, G., and Di Fiore, P. P. (2010) The endocytic matrix. *Nature*. **463**, 464–473

4. Sabharanjak, S., Sharma, P., Parton, R. G., and Mayor, S. (2002) GPI-anchored proteins are delivered to recycling endosomes via a distinct cdc42-regulated, clathrin-independent pinocytic pathway. *Dev. Cell*. **2**, 411–423

5. Maldonado-Báez, L., Cole, N. B., Krämer, H., and Donaldson, J. G. (2013) Microtubule-dependent endosomal sorting of clathrin-independent cargo by Hook1. *J. Cell Biol.* **201**, 233–247

6. Grant, B. D., and Donaldson, J. G. (2009) Pathways and mechanisms of endocytic recycling. *Nat. Rev. Mol. Cell Biol.* **10**, 597–608

7. Mayor, S., and Pagano, R. E. (2007) Pathways of clathrin-independent endocytosis. *Nat. Rev. Mol. Cell Biol.* **8**, 603–612

8. Hattula, K., Furuhjelm, J., Tikkanen, J., Tanhuanpää, K., Laakkonen, P., and Peränen, J. (2006) Characterization of the Rab8-specific membrane traffic route linked to protrusion formation. *J. Cell Sci.* **119**, 4866–4877

9. Eyster, C. A., Higginson, J. D., Huebner, R., Porat-Shliom, N., Weigert, R., Wu, W. W., Shen, R. F., and Donaldson, J. G. (2009) Discovery of new cargo proteins that enter cells through clathrin-independent endocytosis. *Traffic*. **10**, 590–599

10. Fukuda, M. (2008) Membrane traffic in the secretory pathway: Regulation of secretory vesicle traffic by Rab small GTPases. *Cell. Mol. Life Sci.* **65**, 2801–2813

11. Stenmark, H. (2009) Rab GTPases as coordinators of vesicle traffic. *Nat. Rev. Mol. Cell Biol.* **10**, 513–525

12. Pfeffer, S. R. (2013) Rab GTPase regulation of membrane identity. *Curr. Opin. Cell Biol.* **25**, 414–419

13. Barr, F. A. (2013) Rab GTPases and membrane identity: causal or inconsequential? *J. Cell Biol.* **202**, 191–199

14. Sharma, M., Giridharan, S. S. P., Rahajeng, J., Naslavsky, N., and Caplan, S. (2009) MICAL-L1 links EHD1 to tubular recycling endosomes and regulates receptor recycling. *Mol. Biol. Cell.* **20**, 5181–5194

15. Solis, G. P., Hülsbusch, N., Radon, Y., Katanaev, V. L., Plattner, H., and Stuermer, C. A. O. (2013) Reggies/flotillins interact with Rab11a and SNX4 at the tubulovesicular recycling compartment and function in transferrin receptor and E-cadherin trafficking. *Mol. Biol. Cell.* **24**, 2689–2702

16. Weigert, R., Yeung, A. C., Li, J., and Donaldson, J. G. (2004) Rab22a regulates the recycling of membrane proteins internalized independently of clathrin. *Mol. Biol. Cell.* **15**, 3758–3770

17. Rahajeng, J., Panapakkam Giridharan, S. S., Cai, B., Naslavsky, N., and Caplan, S. (2012) MICAL-L1 is a tubular endosomal membrane hub that connects Rab35 and Arf6 with Rab8a. *Traffic.* **13**, 82–93

18. Itoh, T., Fujita, N., Kanno, E., Yamamoto, A., Yoshimori, T., and Fukuda, M. (2008) Golgi-resident small GTPase Rab33B interacts with Atg16L and modulates autophagosome formation. *Mol. Biol. Cell.* **19**, 2916–2925

19. Fukuda, M., and Mikoshiba, K. (1999) A novel alternatively spliced variant of synaptotagmin VI lacking a transmembrane domain: Implications for distinct functions of the two isoforms. *J. Biol. Chem.* **274**, 31428–31434

20. Saitoh, T., Nakayama, M., Nakano, H., Yagita, H., Yamamoto, N., and Yamaoka, S. (2003) TWEAK induces NF-κB2 p100 processing and long lasting NF-κB activation. *J. Biol. Chem.* **278**, 36005–36012

21. Itoh, T., Satoh, M., Kanno, E., and Fukuda, M. (2006) Screening for target Rabs of TBC (Tre-2/Bub2/Cdc16) domain-containing proteins based on their Rab-binding activity. *Genes to Cells*. **11**, 1023–1037

22. Ishida, M., Ohbayashi, N., and Fukuda, M. (2015) Rab1A regulates anterograde melanosome transport by recruiting kinesin-1 to melanosomes through interaction with SKIP. *Sci. Rep*. **5**, 8238

23. Katoh, Y., Nozaki, S., Hartanto, D., Miyano, R., and Nakayama, K. (2015) Architectures of multisubunit complexes revealed by a visible immunoprecipitation assay using fluorescent fusion proteins. *J. Cell Sci*. **128**, 2351–2362

24. Morita, S., Kojima, T., and Kitamura, T. (2000) Plat-E: An efficient and stable system for transient packaging of retroviruses. *Gene Ther*. **7**, 1063–1066

25. Kuroda, T. S., and Fukuda, M. (2005) Identification and biochemical analysis of Slac2-c/MyRIP as a Rab27A-, myosin Va/VIIa-, and actin-binding protein. *Methods Enzymol*. **403**, 431–444

26. Kuki, H., Higaki, T., Yokoyama, R., Kuroha, T., Shinohara, N., Hasezawa, S., and Nishitani, K. (2017) Quantitative confocal imaging method for analyzing cellulose dynamics during cell wall regeneration in Arabidopsis mesophyll protoplasts. *Plant Direct*. **1**, e00021

27. Šali, A., and Blundell, T. L. (1993) Comparative protein modelling by satisfaction of spatial restraints. *J. Mol. Biol*. **234**, 779–815

28. Pettersen, E. F., Goddard, T. D., Huang, C. C., Couch, G. S., Greenblatt, D. M., Meng, E. C., and Ferrin, T. E. (2004) UCSF Chimera--a visualization system for exploratory research and analysis. *J. Comput. Chem*. **25**, 1605–1612

29. Chavrier, P., Parton, R. G., Hauri, H. P., Simons, K., and Zerial, M. (1990) Localization of low-molecular-weight GTP binding-proteins to exocytic and endocytic compartments. *Cell*. **62**, 317–329

30. Peränen, J. (2011) Rab8 GTPase as a regulator of cell shape. *Cytoskeleton*. **68**,

527–539

31. Babbey, C. M., Ahktar, N., Wang, E., Chen, C. C.-H., Grant, B. D., and Dunn, K. W. (2006) Rab10 regulates membrane transport through early endosomes of polarized Madin-Darby canine kidney cells. *Mol. Biol. Cell.* **17**, 3156–3175

32. Ullrich, O., Reinsch, S., Urbé, S., Zerial, M., and Parton, R. G. (1996) Rab11 regulates recycling through the pericentriolar recycling endosome. *J. Cell Biol.* **135**, 913–924

33. Yamamura, R., Nishimura, N., Nakatsuji, H., Arase, S., and Sasaki, T. (2008) The interaction of JRAB/MICAL-L2 with Rab8 and Rab13 coordinates the assembly of tight junctions and adherens junctions. *Mol. Biol. Cell.* **19**, 971–983

34. Hunziker, W., and Peters, P. J. (1998) Rab17 localizes to recycling endosomes and regulates receptor-mediated transcytosis in epithelial cells. *J. Biol. Chem.* **273**, 15734–15741

35. Simpson, J. C. (2004) A role for the small GTPase Rab21 in the early endocytic pathway. *J. Cell Sci.* **117**, 6297–6311

36. Kauppi, M., Simonsen, A., Bremnes, B., Vieira, A., Callaghan, J., Stenmark, H., and Olkkonen, V. M. (2002) The small GTPase Rab22 interacts with EEA1 and controls endosomal membrane trafficking. *J. Cell Sci.* **115**, 899–911

37. Evans, T. M., Ferguson, C., Wainwright, B. J., Parton, R. G., and Wicking, C. (2003) Rab23, a negative regulator of hedgehog signaling, localizes to the plasma membrane and the endocytic pathway. *Traffic.* **4**, 869–884

38. Mrozowska, P. S., and Fukuda, M. (2016) Regulation of podocalyxin trafficking by Rab small GTPases in 2D and 3D epithelial cell cultures. *J. Cell Biol.* **213**, 355–369

39. Liu, Y., Xu, X.-H., Chen, Q., Wang, T., Deng, C.-Y., Song, B.-L., Du, J.-L., and Luo, Z.-G. (2013) Myosin Vb controls biogenesis of post-Golgi Rab10 carriers during axon development. *Nat. Commun.* **4**, 2005

40. English, A. R., and Voeltz, G. K. (2013) Rab10 GTPase regulates ER dynamics

and morphology. *Nat. Cell Biol.* **15**, 169–178

41. Chen, Y., Gershlick, D. C., Park, S. Y., and Bonifacino, J. S. (2017) Segregation in the Golgi complex precedes export of endolysosomal proteins in distinct transport carriers. *J. Cell Biol.* **216**, 4141–4151

42. Nakajo, A., Yoshimura, S. ichiro, Togawa, H., Kunii, M., Iwano, T., Izumi, A., Noguchi, Y., Watanabe, A., Goto, A., Sato, T., and Harada, A. (2016) EHBP1L1 coordinates Rab8 and Bin1 to regulate apical-directed transport in polarized epithelial cells. *J. Cell Biol.* **212**, 297–306

43. Wang, P., Liu, H., Wang, Y., Liu, O., Zhang, J., Gleason, A., Yang, Z., Wang, H., Shi, A., and Grant, B. D. (2016) RAB-10 promotes EHBP-1 bridging of filamentous actin and tubular recycling endosomes. *PLoS Genet.* **12**, e1006093

44. Faire, K., Waterman-Storer, C. M., Gruber, D., Masson, D., Salmon, E. D., and Bulinski, J. C. (1999) E-MAP-115 (ensconsin) associates dynamically with microtubules in vivo and is not a physiological modulator of microtubule dynamics. *J. Cell Sci.* **112**, 4243–4255

45. Rai, A., Oprisko, A., Campos, J., Fu, Y., Friese, T., Itzen, A., Goody, R. S., Gazdag, E. M., and Müller, M. P. (2016) bMERB domains are bivalent Rab8 family effectors evolved by gene duplication. *Elife.* **5**, e18675

46. Chen, Y., Wang, Y., Zhang, J., Deng, Y., Jiang, L., Song, E., Wu, X. S., Hammer, J. A., Xu, T., and Lippincott-Schwartz, J. (2012) Rab10 and myosin-Va mediate insulin-stimulated GLUT4 storage vesicle translocation in adipocytes. *J. Cell Biol.* **198**, 545–560

47. Deng, C.-Y., Lei, W.-L., Xu, X.-H., Ju, X.-C., Liu, Y., and Luo, Z.-G. (2014) JIP1 mediates anterograde transport of Rab10 cargos during neuronal polarization. *J. Neurosci.* **34**, 1710–1723

48. Bruno, J., Brumfield, A., Chaudhary, N., Iaea, D., and McGraw, T. E. (2016) SEC16A is a RAB10 effector required for insulin-stimulated GLUT4 trafficking in adipocytes. *J. Cell Biol.* **214**, 61–76

49. Fukuda, M., Kanno, E., Ishibashi, K., and Itoh, T. (2008) Large scale screening for novel Rab effectors reveals unexpected broad Rab binding specificity. *Mol. Cell. Proteomics*. **7**, 1031–1042

50. Wang, T., Liu, Y., Xu, X. H., Deng, C. Y., Wu, K. Y., Zhu, J., Fu, X. Q., He, M., and Luo, Z. G. (2011) Lgl1 activation of Rab10 promotes axonal membrane trafficking underlying neuronal polarization. *Dev. Cell*. **21**, 431–444

51. Miki, H., Okada, Y., and Hirokawa, N. (2005) Analysis of the kinesin superfamily: Insights into structure and function. *Trends Cell Biol*. **15**, 467–476

52. Soppina, V., Norris, S. R., Dizaji, A. S., Kortus, M., Veatch, S., Peckham, M., and Verhey, K. J. (2014) Dimerization of mammalian kinesin-3 motors results in superprocessive motion. *Proc. Natl. Acad. Sci*. **111**, 5562–5567

53. Du, W., Su, Q. P., Chen, Y., Zhu, Y., Jiang, D., Rong, Y., Zhang, S., Zhang, Y., Ren, H., Zhang, C., Wang, X., Gao, N., Wang, Y., Sun, L., Sun, Y., and Yu, L. (2016) Kinesin 1 drives autolysosome tubulation. *Dev. Cell*. **37**, 326–336

54. Zhou, R., Niwa, S., Guillaud, L., Tong, Y., and Hirokawa, N. (2013) A molecular motor, KIF13A, controls anxiety by transporting the serotonin type 1A receptor. *Cell Rep*. **3**, 509–519

55. Radhakrishna, H., and Donaldson, J. G. (1997) ADP-ribosylation factor 6 regulates a novel plasma membrane recycling pathway. *J. Cell Biol*. **139**, 49–61

56. Caplan, S., Naslavsky, N., Hartnell, L. M., Lodge, R., Polishchuk, R. S., Donaldson, J. G., and Bonifacino, J. S. (2002) A tubular EHD1-containing compartment involved in the recycling of major histocompatibility complex class I molecules to the plasma membrane. *EMBO J*. **21**, 2557–2567

57. Sakane, A., Abdallah, A. A. M., Nakano, K., Honda, K., Ikeda, W., Nishikawa, Y., Matsumoto, M., Matsushita, N., Kitamura, T., and Sasaki, T. (2012) Rab13 small G protein and junctional Rab13-binding protein (JRAB) orchestrate actin cytoskeletal organization during epithelial junctional development. *J. Biol. Chem*. **287**, 42455–42468

58. Chaineau, M., Ioannou, M. S., and Mcpherson, P. S. (2013) Rab35: GEFs, GAPs and Effectors. *Traffic*. **14**, 1109–1117

59. Condon, N. D., Heddleston, J. M., Chew, T.-L., Luo, L., McPherson, P. S., Ioannou, M. S., Hodgson, L., Stow, J. L., and Wall, A. A. (2018) Macropinosome formation by tent pole ruffling in macrophages. *J. Cell Biol.* **217**, 3873–3885

60. Dutta, D., and Donaldson, J. G. (2015) Sorting of clathrin-independent cargo proteins depends on Rab35 delivered by clathrin-mediated endocytosis. *Traffic*. **16**, 994–1009

61. Zacchi, P., Stenmark, H., Parton, R. G., Orioli, D., Lim, F., Giner, A., Mellman, I., Zerial, M., and Murphy, C. (1998) Rab17 regulates membrane trafficking through apical recycling endosomes in polarized epithelial cells. *J. Cell Biol.* **140**, 1039–1053

62. Delevoye, C., Miserey-Lenkei, S., Montagnac, G., Gilles-Marsens, F., Paul-Gilloteaux, P., Giordano, F., Waharte, F., Marks, M., Goud, B., and Raposo, G. (2014) Recycling endosome tubule morphogenesis from sorting endosomes requires the kinesin motor KIF13A. *Cell Rep.* **6**, 445–454

63. Gong, Q., Weide, M., Huntsman, C., Xu, Z., Jan, L. Y., and Ma, D. (2007) Identification and characterization of a new class of trafficking motifs for controlling clathrin-independent internalization and recycling. *J. Biol. Chem.* **282**, 13087–13097

64. Navarro Negredo, P., Edgar, J. R., Wrobel, A. G., Zaccai, N. R., Antrobus, R., Owen, D. J., and Robinson, M. S. (2017) Contribution of the clathrin adaptor AP-1 subunit μ1 to acidic cluster protein sorting. *J. Cell Biol.* **216**, 2927–2943

65. Lv, P., Sheng, Y., Zhao, Z., Zhao, W., Gu, L., Xu, T., and Song, E. (2015) Targeted disruption of Rab10 causes early embryonic lethality. *Protein Cell*. **6**, 463–467

66. Zhang, Z. huan, Zhao, W. Q., Ma, F. fei, Zhang, H., and Xu, X. H. (2017) Rab10 disruption results in delayed OPC maturation. *Cell. Mol. Neurobiol.* **37**,

1303–1310

67. Vazirani, R. P., Verma, A., Sadacca, L. A., Buckman, M. S., Picatoste, B., Beg, M., Torsitano, C., Bruno, J. H., Patel, R. T., Simonyte, K., Camporez, J. P., Moreira, G., Falcone, D. J., Accili, D., Elemento, O., Shulman, G. I., Kahn, B. B., and McGraw, T. E. (2016) Disruption of adipose Rab10-dependent insulin signaling causes hepatic insulin resistance. *Diabetes*. **65**, 1577–1589

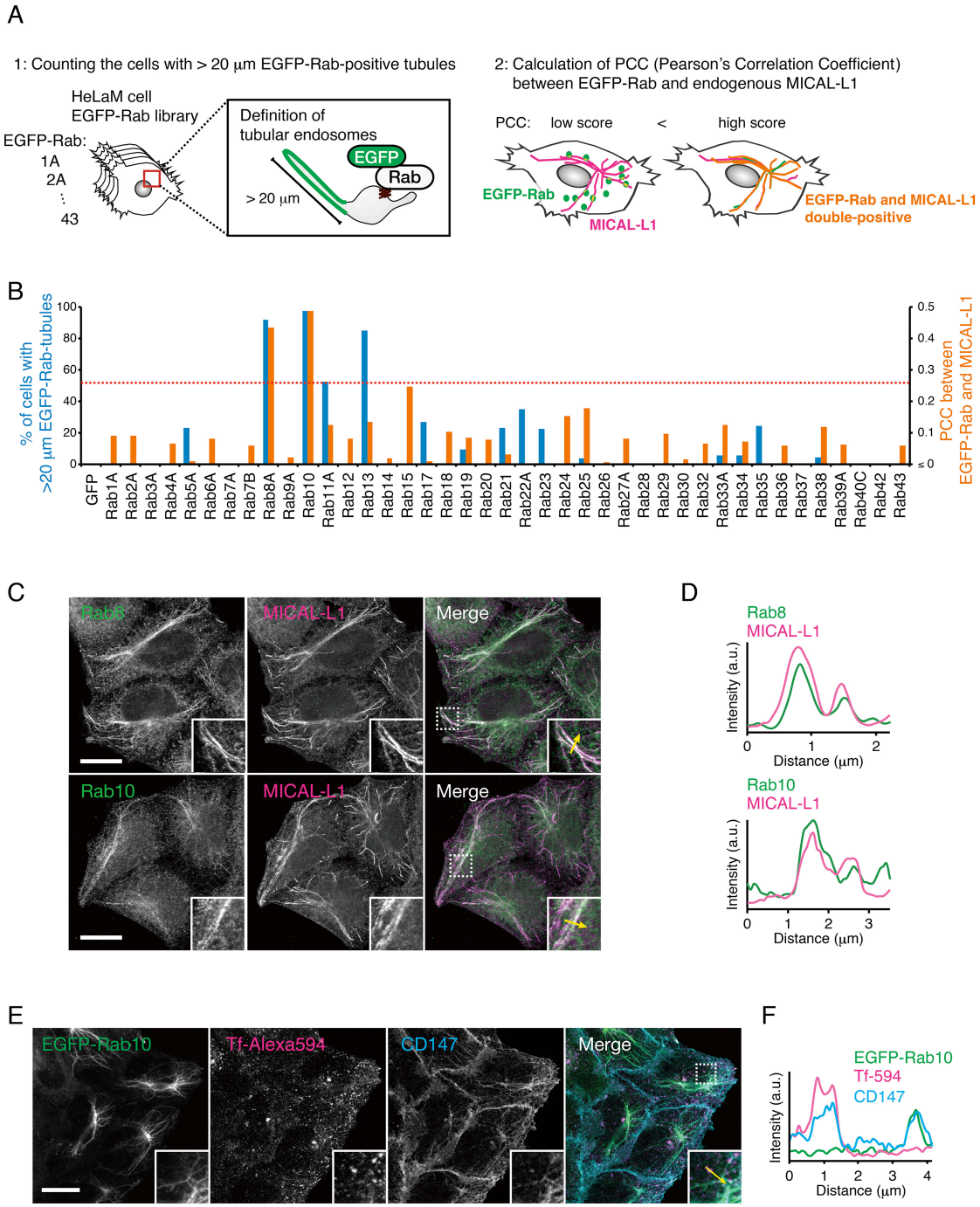

FIGURE 1. Rab8 and Rab10 are mainly localized at tubular endosomes.

(A) Schematic representation of the method used to screen for Rabs that are mainly localized at tubular endosomes. In the first step, a library of HeLaM cells stably expressing EGFP-Rabs (Rab1A–43) was analyzed for the presence of at least one EGFP-positive tubular structure >20 μm in length (blue bars in B). In the second step,

EGFP-Rab-expressing HeLaM cells were immunostained with antibody against MICAL-L1 (a tubular endosome marker), and then PCCs for the relation between EGFP-Rabs and MICAL-L1 were calculated (orange bars in B).

(B) Quantification of the results of the first step (A-1, blue bars) and the second step (A-2, orange bars). The red line represents quadruple the median PCC value, and it was used as a threshold for tubular-endosome-localization of Rabs.

(C) Colocalization between Rab8 (green, upper panels) and Rab10 (green, lower panels) and MICAL-L1 (magenta) at the endogenous protein level. The insets are magnified views of the boxed areas. Scale bars, 20 μm.

(D) Line plot profiles of the yellow arrows in the insets in C.

(E) Localization of EGFP-Rab10 (green), internalized Alexa594-Tf (magenta), and internalized anti-CD147 (cyan) in HeLaM cells. HeLaM cells stably expressing EGFP-Rab10 were incubated for 2 h at 37°C with both 5 μg/ml Alexa594-Tf and 5 μg/ml anti-CD147 antibody. The insets are magnified views of the boxed areas. Scale bars, 20 μm.

(F) Line plot profiles of the yellow arrows in the insets in E.

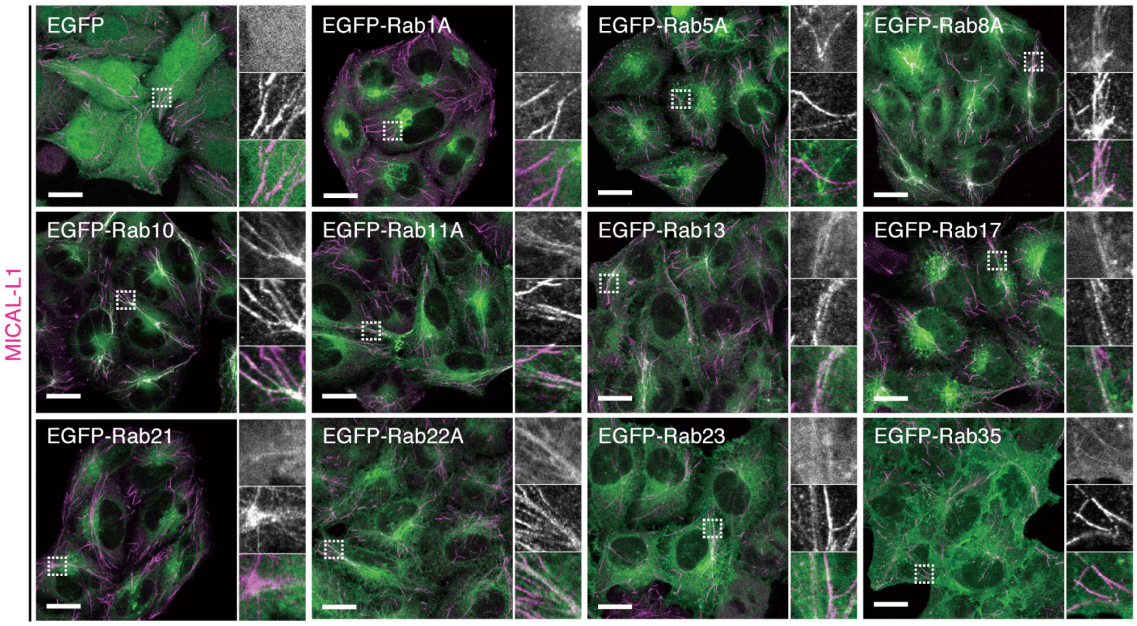

FIGURE 2. A localization screen uncovers tubular endosome-resident Rabs. Localization of EGFP-Rabs (Rab5A, 8A, 10, 11A, 13, 17, 21, 22A, 23, and 35) (green) on tubular endosomes in HeLaM cells. HeLaM cells stably expressing EGFP or EGFP-Rab (1A, 5A, 8A, 10, 11A, 13, 17, 21, 22A, 23, or 35) (green) were immunostained with the anti-MICAL-L1 antibody (magenta). The insets are magnified views of the boxed areas. Scale bars, 20 μm.

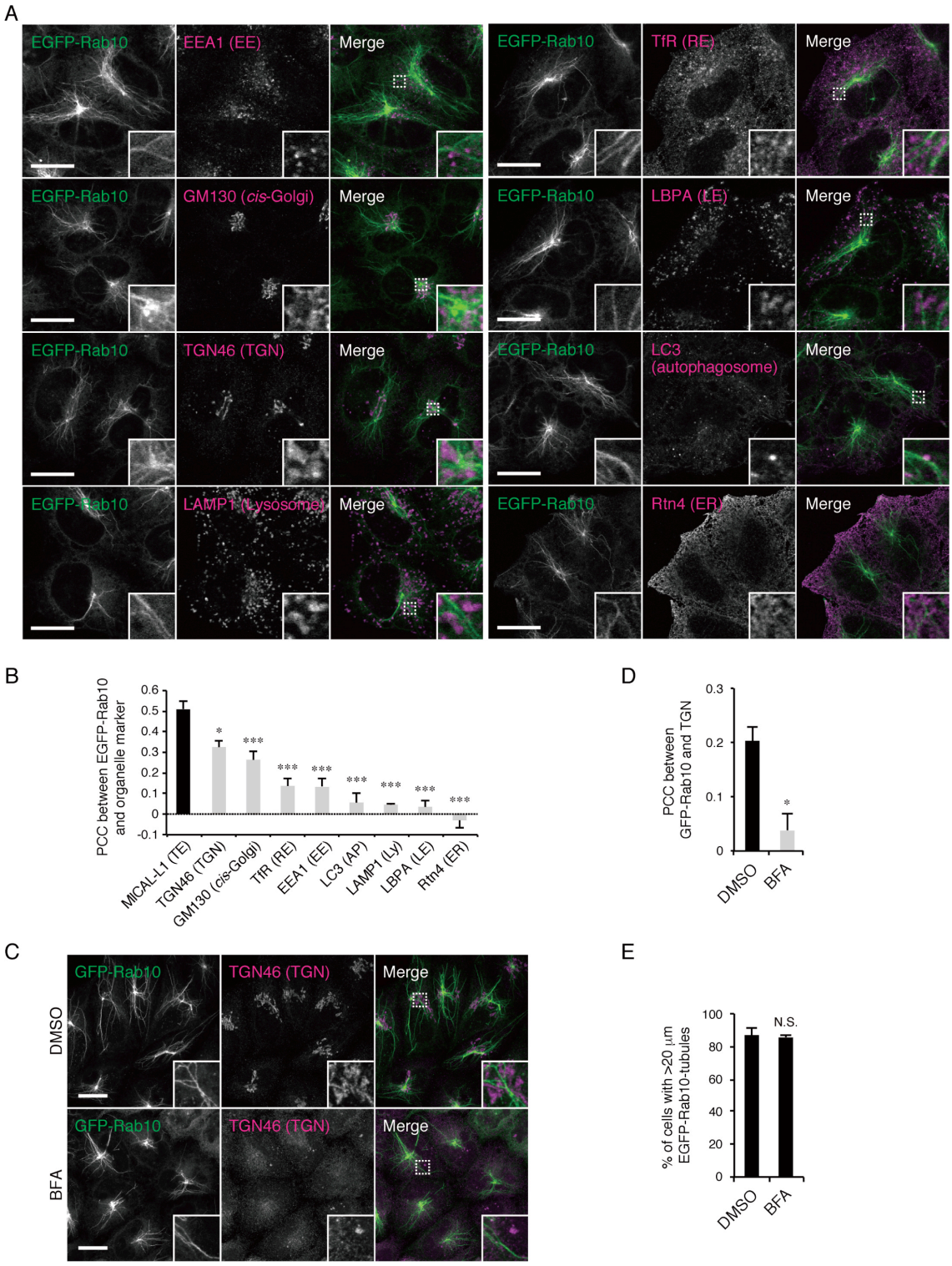

FIGURE 3. EGFP-Rab10 is mainly localized at tubular endosomes.

(A) Subcellular localization of EGFP-Rab10 in HeLaM cells. HeLaM cells stably expressing EGFP-Rab10 (green) were immunostained with antibodies against EEA1

(EE), GM130 (*cis*-Golgi), TGN46 (TGN), LAMP1 (lysosome), TfR (RE), LBPA (LE), LC3 (autophagosome), and Rtn4 (ER) (magenta). The insets are magnified views of the boxed areas. Scale bars, 20 μm.

(B) PCCs for the relation between EGFP-Rab10 and the organelle markers shown in A. The bars represent the means and SEM of data from three independent experiments (n = 3; more than 4 images were analyzed in each experiment). ∗, $p < 0.05$; ∗∗∗, $p < 0.001$ (Dunnett's test).

(C) Subcellular localization of EGFP-Rab10 in DMSO- and BFA-treated HeLaM cells. HeLaM cells stably expressing EGFP-Rab10 (green) were treated with DMSO or 1 μg/ml BFA for 1 h before fixation and immunostained with anti-TGN46 antibody (magenta). The insets are magnified views of the boxed areas. Scale bars, 20 μm.

(D) PCCs for the relation between EGFP-Rab10 and TGN46 shown in C. The bars represent the means and SEM of data from three independent experiments (n = 3; more than 4 images were analyzed in each experiment). ∗, $p < 0.05$ (unpaired two-tailed Student's *t* test).

(E) Percentages of cells containing at least one EGFP-Rab10-positive tubule >20 μm in length shown in C. The bars represent the means and SEM of data from three independent experiments (n = 3; more than 20 cells were analyzed in each experiment).

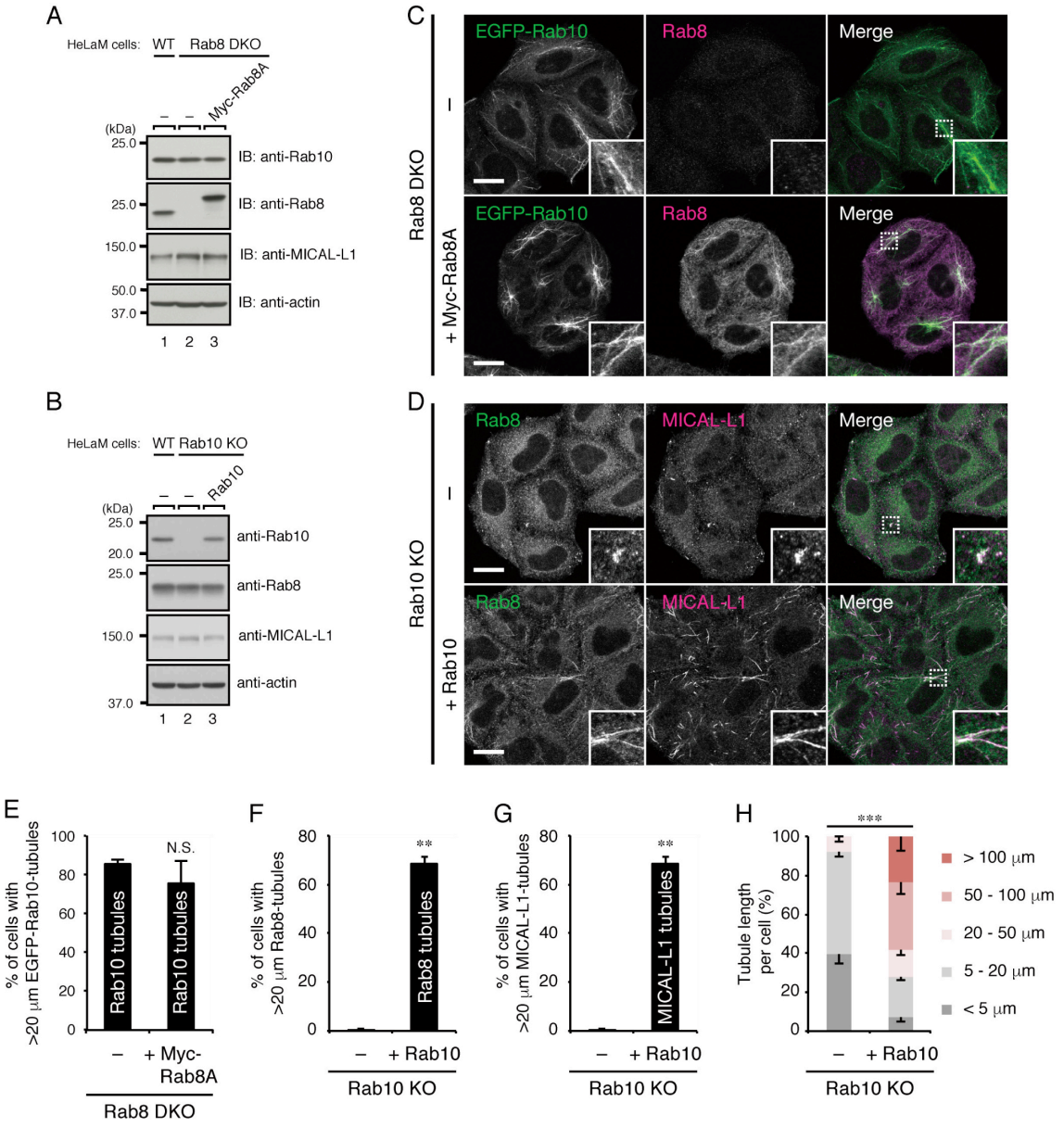

FIGURE 4. Rab10, not Rab8, is essential for tubular endosome formation.

(A and B) Rab8A/B double knockout (DKO) and Rab10 knockout (KO) HeLaM cells generated by the CRISPR/Cas9 system. Cell lysates of parental cells, Rab8-DKO cells, Rab8-DKO cells stably expressing Myc-tagged Rab8A (Rab8-DKO + Myc-Rab8A) cells (A), Rab10-KO cells, and Rab10-KO cells stably expressing Rab10 (Rab10-KO + Rab10) cells (B) were analyzed by immunoblotting with the antibodies indicated.

(C and D) Tubular endosomes in Rab8-DKO cells (C) and Rab10-KO cells (D). Rab8-DKO cells and Rab8-DKO + Myc-Rab8A cells stably expressing EGFP-Rab10 were immunostained with anti-Rab8 antibody (C). Rab10-KO cells and Rab10-KO +

Rab10 cells were immunostained with antibodies against Rab8 and MICAL-L1 (D). The insets are magnified views of the boxed areas. Scale bars, 20 μm.

(E) Quantification of the percentages of cells containing at least one EGFP-Rab10-tubule >20 μm in length. (F) Quantification of the percentages of cells containing at least one Rab8-tubule >20 μm in length. (G) Quantification of the percentages of cells containing at least one MICAL-L1-tubule >20 μm in length. The bars represent the means and SEM of data from three independent experiments (n = 3; more than 20 cells were analyzed in each experiment). ***, $p < 0.001$ (unpaired two-tailed Student's *t* test).

(H) Histogram analysis of the length of MICAL-L1-positive tubules in Rab10-KO cells and Rab10-KO + Rab10 cells. Total tubule length (i.e., the sum of the length of all tubules) in individual cells was classified into five categories: "<5 μm", "5–20 μm", "20–50 μm", "50–100 μm", or ">100 μm", and the number of cells containing tubules having the total tubule length in each category was counted as described in the Materials and Methods. The numbers of cells in each category as percentages of the total cell population are expressed as stacked bar graphs. The bars represent the means and SEM of data from three independent experiments (n = 3; more than 30 cells were analyzed in each experiment). ***, $p < 0.001$ (Pearson's χ^2 test).

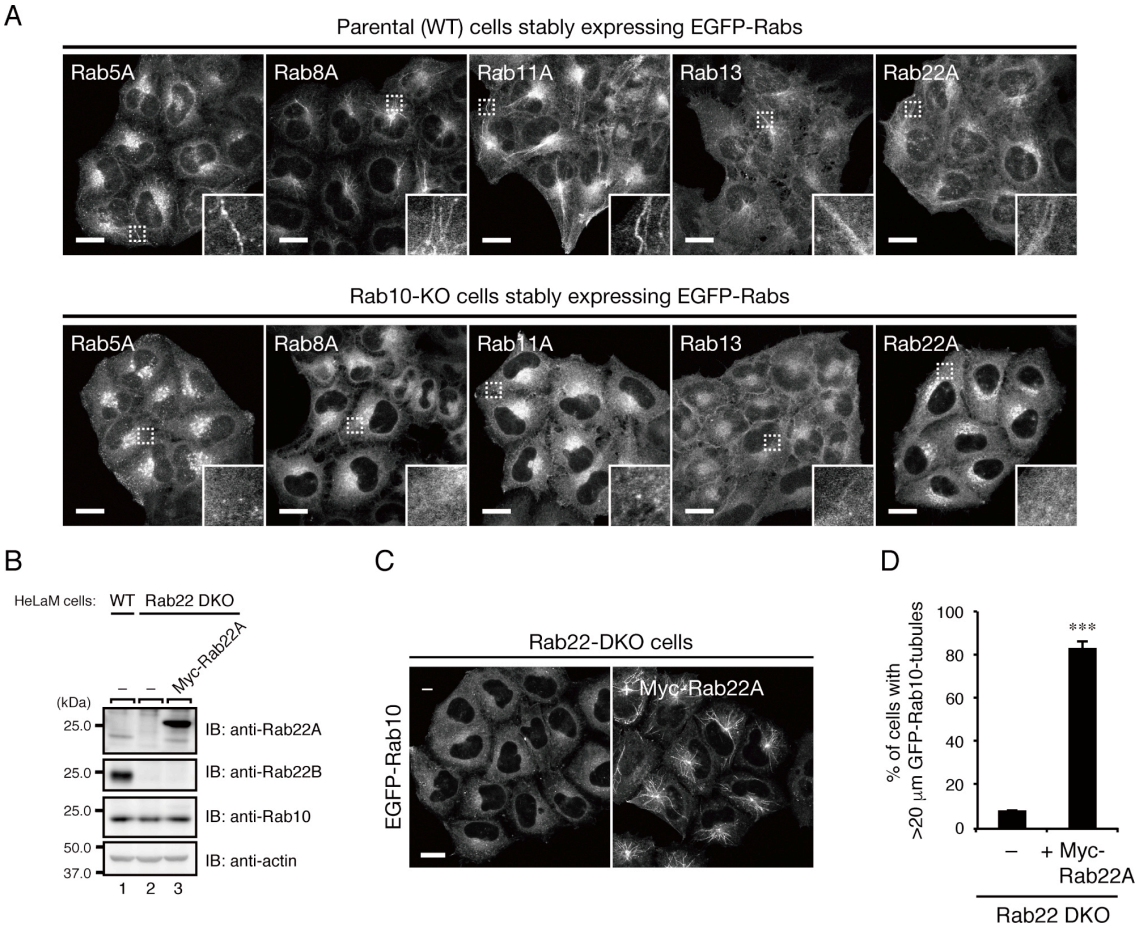

FIGURE 5. Both Rab10 and Rab22A/B are necessary for tubular endosome formation.

(A) Localization of the tubular-endosome-resident Rabs (Rab5A, 8A, 11A, 13, and 22A) in WT and Rab10-KO HeLaM cells. WT and Rab10-KO cells stably expressing EGFP-Rab (Rab5A, 8A, 11A, 13, or 22A) were observed. The insets are magnified views of the boxed areas. Scale bars, 20 μm.

(B) Rab22A/B double knockout (DKO) HeLaM cells generated by the CRISPR/Cas9 system. Cell lysates of parental cells, Rab22-DKO cells, and Rab22-DKO cells stably expressing Myc-tagged Rab22A (Rab22-DKO + Myc-Rab22A) cells were analyzed by immunoblotting with the antibodies indicated.

(C) Tubular endosomes in Rab22-DKO cells. Rab22-DKO cells and Rab22-DKO + Myc-Rab22A cells stably expressing EGFP-Rab10 were observed. The insets are magnified views of the boxed areas. Scale bar, 20 μm.

(D) Percentages of cells containing at least one EGFP-Rab10-positive tubule >20 mm in

length shown in C. The bars represent the means and SEM of data from three independent experiments (n = 3; more than 30 cells were analyzed in each experiment). ***, $p < 0.001$ (unpaired two-tailed Student's *t* test).

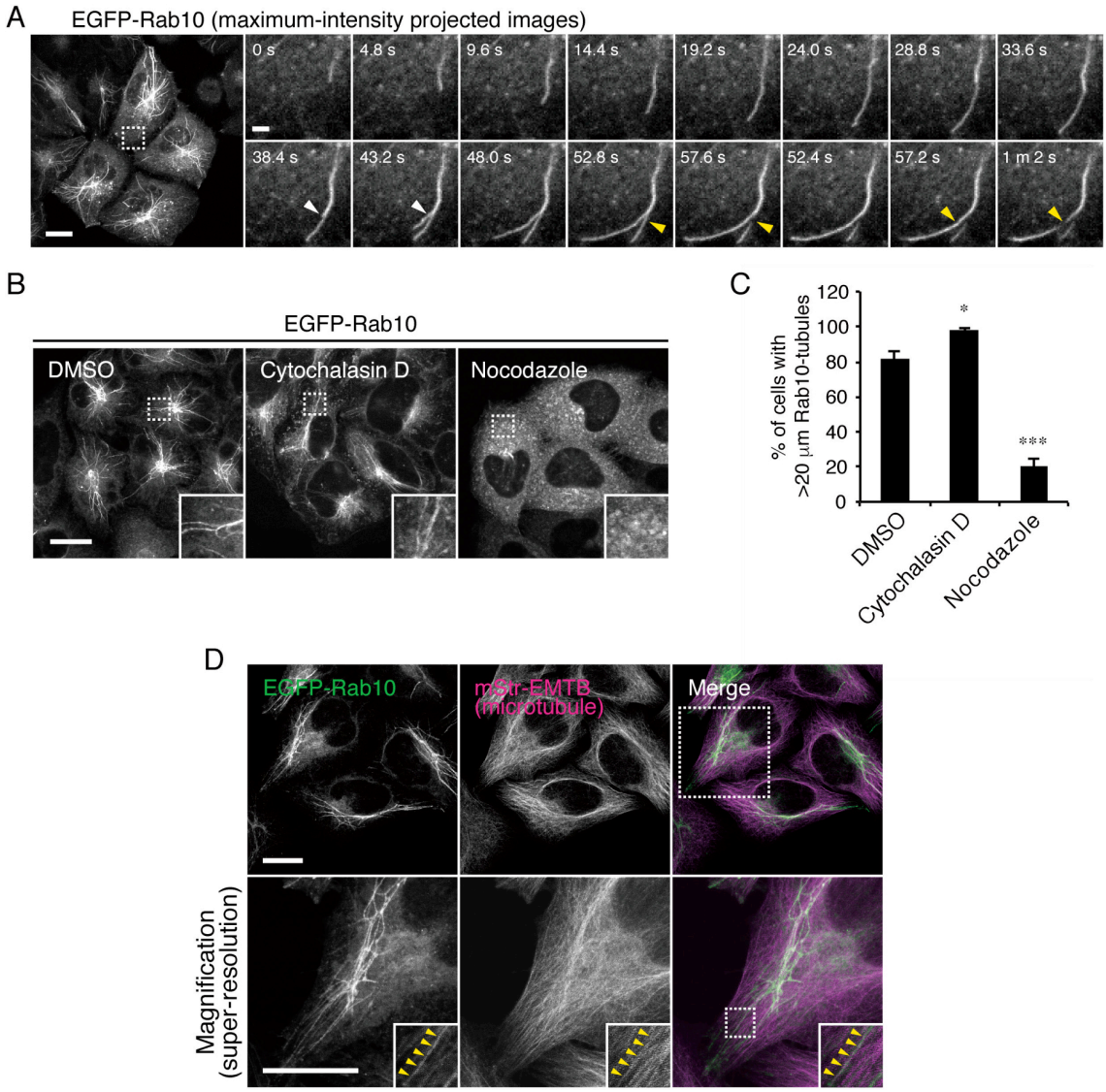

FIGURE 6. Microtubules are necessary for tubular endosome extension.

(A) Dynamics of EGFP-Rab10-positive tubules. HeLaM cells stably expressing EGFP-Rab10 were analyzed by live-cell imaging on a spinning-disk confocal microscope. Image stacks of the regions of interest were captured, and maximum intensity projections were obtained. The time-lapse images of the boxed area captured at 4.8 s intervals are shown on the right. Arrowheads point to the fission sites of tubular endosomes. Scale bars in the whole image and in the insets, 20 μm and 2 μm, respectively.

(B) Effect of DMSO (control), cytochalasin D, and nocodazole on EGFP-Rab10-positive tubules. HeLaM cells stably expressing EGFP-Rab10 were treated for 1 h with 0.1% DMSO, 10 μM cytochalasin D, or 10 μg/ml nocodazole.

The insets are magnified views of the boxed areas. Scale bar, 20 μm. $*, p < 0.05$; $***, p < 0.001$ (Dunnett's test).

(C) Percentages of cells containing EGFP-Rab10-positive tubules shown in B. The bars represent the means and SEM of data from three independent experiments (n = 3; more than 20 cells were analyzed in each experiment).

(D) Colocalization between EGFP-Rab10 and mStr-EMTB (a microtubule marker). Typical images of HeLaM cells stably co-expressing EGFP-Rab10 and mStr-EMTB were captured with a conventional confocal microscope (upper panels) or OSR (Olympus Super Resolution; lower panels). The super-resolution images correspond to the boxed area in the upper left panel. The insets in the lower panels are magnified views of the boxed areas. Arrowheads point to a microtubule and EGFP-Rab10 double-positive tubule. Scale bars, 20 μm.

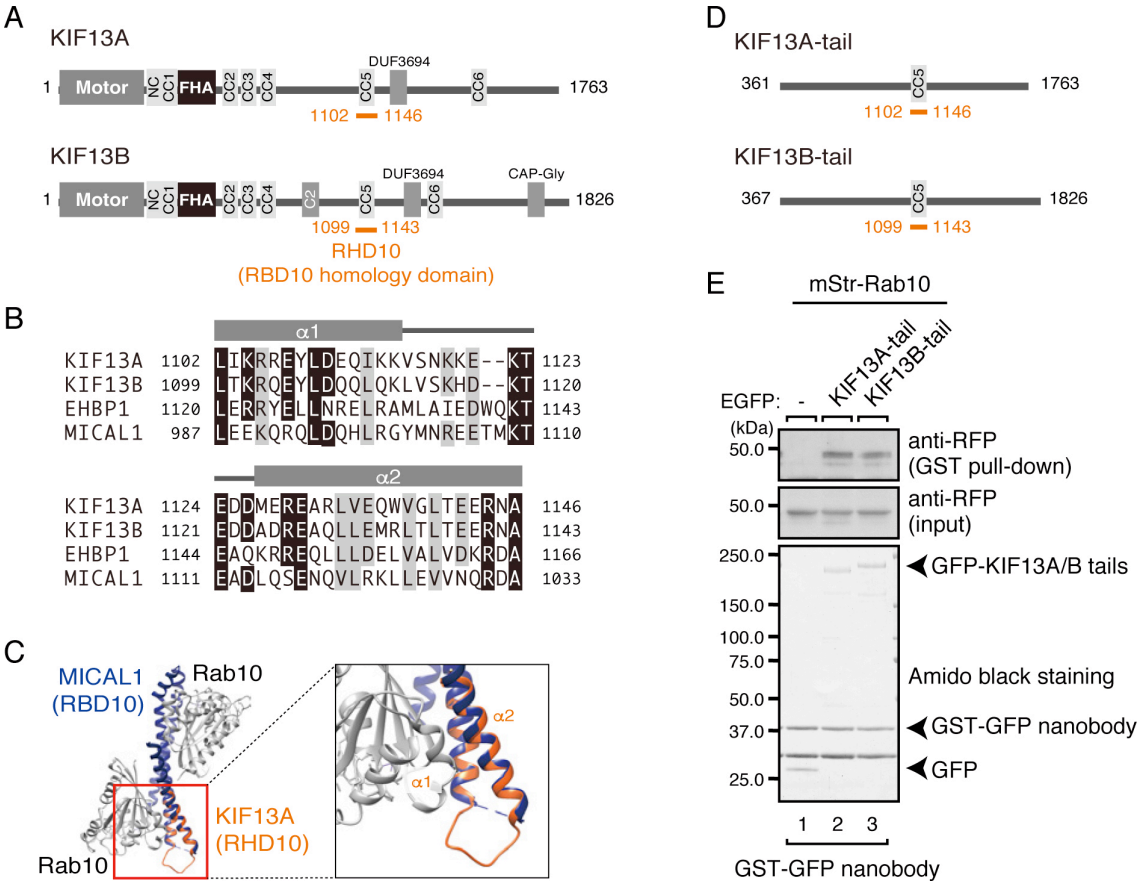

FIGURE 7. KIF13A/B are novel Rab10-interacting proteins.

(A) Schematic representation of mouse KIF13A/B. Amino acid (AA) numbers are shown on both sides of each KIF13 protein. The Rab10-binding homology domain (named RHD10) of KIF13A/B determined in this study is represented by orange lines.

(B) Sequence alignment and predicted secondary structure of the RBD10 or RHD10 of mouse KIF13A/B, EHBP1, and MICAL1. The amino acid residues that are conserved and that are similar in more than three sequences are shown against a black background and against a shaded background, respectively. The predicted secondary structure is indicated above the corresponding sequences.

(C) A 3D-homology model of the KIF13A RHD10 and the crystal structure of the Rab10–MICAL1 (RBD10) complex (PDB: 5LPN). The predicted 3D-structure of the KIF13A RHD10 (orange) is superimposed on the MICAL1 RBD10 (blue) in complex with Rab10 (silver). The α-helix 1 and α-helix 2 in the KIF13A RHD10 of the boxed area correspond to the secondary structure shown in B.

(D) Schematic representation of KIF13A/B-tail mutants without a motor domain.

(E) Interaction between Rab10 and KIF13A/B-tail. mStr-Rab10 and EGFP-KIF13A/B-tail were co-expressed in COS-7 cells, and their associations were analyzed by co-immunoprecipitation assays with glutathione-Sepharose beads coupled with GST-GFP nanobody, followed by immunoblotting with the antibodies indicated.

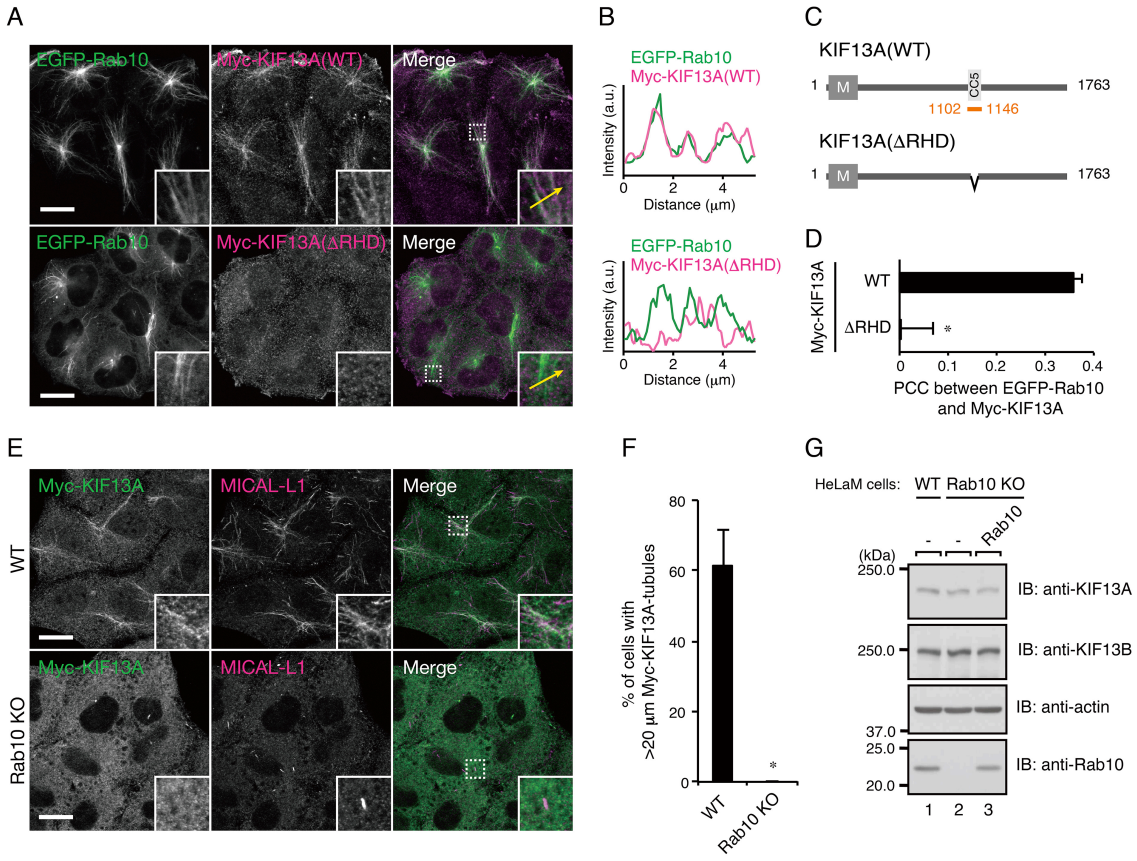

FIGURE 8. The RHD10 of KIF13 is required for its localization at EGFP-Rab10-positive tubules.

(A) Localization of Myc-KIF13A (WT and ΔRHD10). HeLaM cells stably co-expressing EGFP-Rab10 (green) and Myc-KIF13A (WT or ΔRHD10; magenta) were examined. The insets are magnified views of the boxed areas. Scale bars, 20 μm.

(B) Line plot profiles of the yellow arrows in the insets in A.

(C) Schematic representation of a KIF13A(ΔRHD10) mutant that lacks an RHD10 shown in orange.

(D) PCCs for the relation between EGFP-Rab10 and Myc-KIF13A (WT or ΔRHD10) shown in A. The bars represent the means and SEM of data from three independent experiments (n = 3; more than 5 images were analyzed in each experiment). ∗, $p < 0.05$ (unpaired two-tailed Student's *t* test).

(E) Localization of Myc-KIF13A in Rab10-KO cells. Rab10-KO cells stably expressing Myc-KIF13A (green) were immunostained with the anti-MICAL-L1

antibody. The insets are magnified views of the boxed areas. Scale bars, 20 μm.
(F) Percentages of cells containing at least one Myc-KIF13A-positive tubule >20 μm in length shown in E. The bars represent the means and SEM of data from three independent experiments (n = 3; more than 20 cells were analyzed in each experiment). ∗, $p < 0.05$ (unpaired two-tailed Student's *t* test).
(G) Unaltered expression of KIF13A/B in Rab10-KO cells. Cell lysates of parental (WT) cells, Rab10-KO cells, and Rab10-KO cells stably expressing Rab10 (Rab10-KO + Rab10) were analyzed by immunoblotting with the antibodies indicated.

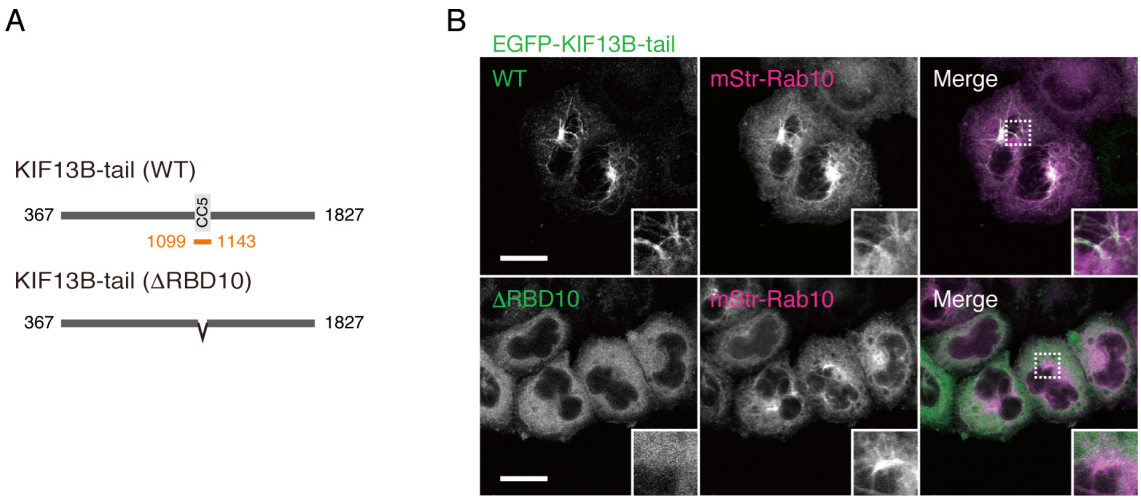

FIGURE 9. The RHD10 of KIF13B is required for its localization at EGFP-Rab10-positive tubules.

(A) Schematic representation of KIF13B-tail (WT and ΔRHD10) mutants.

(B) Localization of EGFP-KIF13B-tail (WT and ΔRHD10). HeLaM cells transiently co-expressing EGFP-KIF13B-tail (WT or ΔRHD10; green) and mStr-Rab10 (magenta) were observed. The insets are magnified views of the boxed areas. Scale bars, 20 μm.

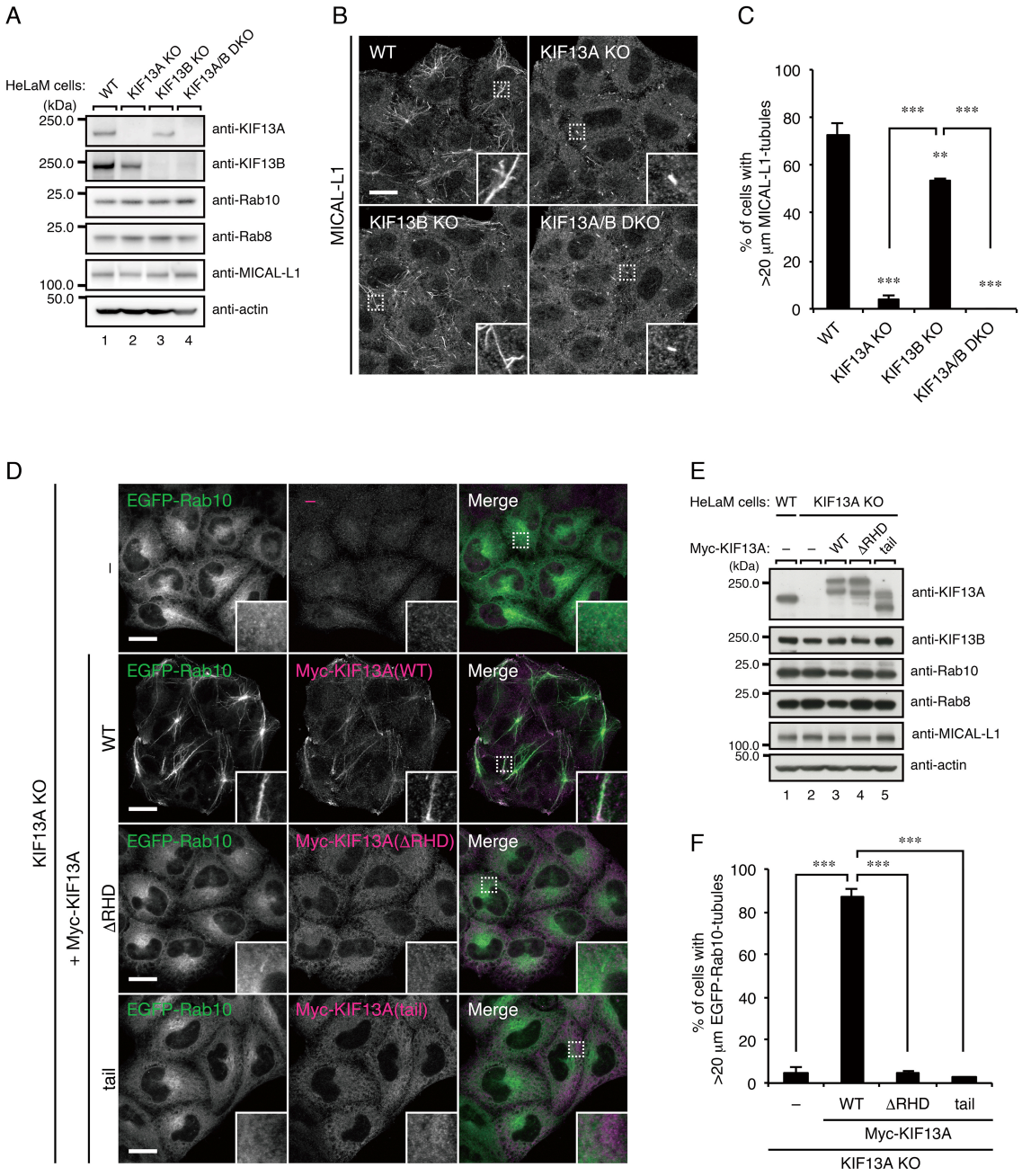

FIGURE 10. Both the motor domain and the RHD10 of KIF13A are necessary for tubular endosome formation.

(A) KIF13A-KO, KIF13B-KO, and KIF13-DKO HeLaM cells generated by the CRISPR/Cas9 system. Cell lysates of parental (WT), KIF13A-KO, KIF13B-KO, and KIF13-DKO cells were analyzed by immunoblotting with the antibodies indicated.

(B) Tubular endosomes in KIF13A-KO, KIF13B-KO, and KIF13-DKO cells. Each cell line was immunostained with the anti-MICAL-L1 antibody. The insets are

magnified views of the boxed areas. Scale bar, 20 μm.

(C) Percentages of cells containing at least one MICAL-L1-positive tubule >20 μm in length shown in B. **, $p < 0.01$; ***, $p < 0.001$ (Dunnett's test).

(D) Rescue of KIF13A-KO cells by exogenous expression of KIF13A mutants. KIF13A-KO cells stably co-expressing EGFP-Rab10 (green) and Myc-KIF13A (WT, ΔRHD10, or tail) (magenta) were tested. The insets are magnified views of the boxed areas. Scale bars, 20 μm.

(E) Similar level of Myc-KIF13A expression (WT, ΔRHD10, or tail) in KIF13A-KO cells. Cell lysates of parental (WT) cells, KIF13A-KO cells, and KIF13A-KO cells stably expressing Myc-KIF13A (WT, ΔRHD10, or tail) were analyzed by immunoblotting with the antibodies indicated.

(F) Percentages of cells containing at least one EGFP-Rab-10-positive tubule >20 μm in length shown in D. The bars represent the means and SEM of data from three independent experiments (n = 3; more than 20 cells were analyzed in each experiment). ***, $p < 0.001$ (one-way analysis of variance followed by the Tukey-Kramer test).

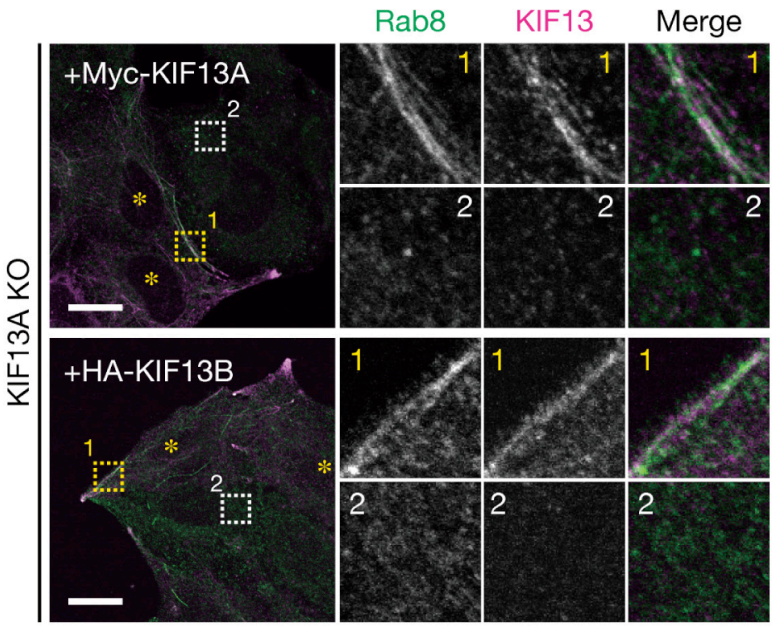

FIGURE 11. Overexpression of HA-KIF13A/B rescued the disruption of tubular endosomes in KIF13A-KO cells.

Tubular endosomes in KIF13A-KO cells transiently expressing HA-KIF13A or HA-KIF13B. The cells were immunostained with antibodies against Rab8 (green) and MICAL-L1 (magenta). The insets are magnified views of the boxed areas. Box 1 (yellow) and Box 2 (white) indicate the cells expressing HA-KIF13 and not expressing HA-KIF13, respectively. Scale bars, 20 μm.

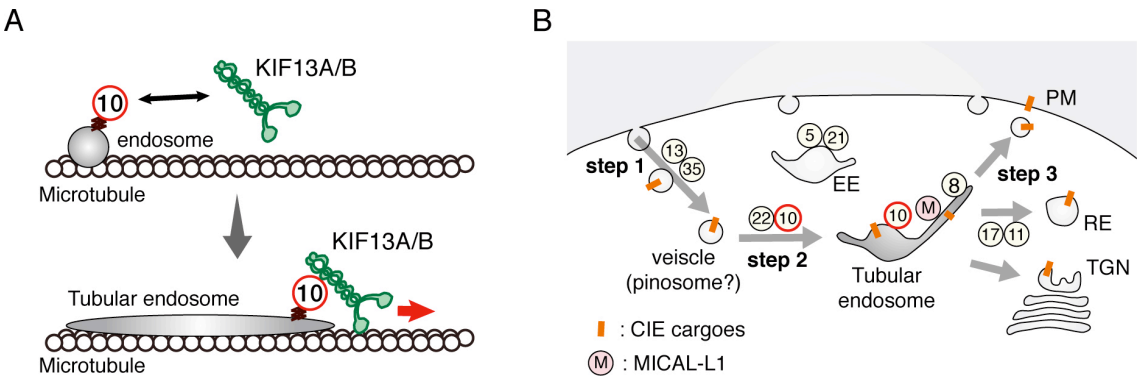

FIGURE 12. Proposed model of the role of Rabs in tubular endosome formation.

(A) In HeLaM cells, Rab10 is localized at endosomes and recruits KIF13 motors to induce endosome tubulation by pulling along a microtubule track.

(B) Proposed model of Rab-mediated tubular endosome formation based on the results obtained in the present study together with previous reports (see Discussions for details). In the first step, CIE cargoes, including CD147, are internalized through the Arf6-dependent pathway (9), and Rab13 and 35 may be involved in this step through actin reorganization (57, 58). In the second step, the internalized vesicle-to-tubular endosome transition occurs (55). Rab10 and 22A/B are necessary to complete this step, and thus KO of either Rab10 or 22A/B caused failure of tubular endosomes to develop. Rab5A and 21, neither of which colocalized with MICAL-L1, may not be directly involved in CIE cargo sorting/transport (4, 63). In the final step, the CIE cargoes in the tubular endosome are sorted and transported into the PM, RE, or TGN (Step 3) (4, 8). Rab8, 11A, and 17 may contribute to this step (15, 42, 61).

Acknowledgements

I achieved this thesis in the Laboratory of Membrane Trafficking Mechanisms, Department of Developmental Biology and Neurosciences, Graduate School of Life Sciences, Tohoku University. I am grateful to Professor Mitsunori Fukuda for appropriate direction and a lot of valuable suggestions. I am also grateful to Assistant Professor Naonobu Fujita and Dr. Yuta Homma for technical advice and critical reading of the manuscript. I have a lot of thankfulness to Dr. Hotaka Kobayashi for teaching me experimental methods and presentation skills, and to Megumi Aizawa, Yuki Hatoyama, Koki Okuyama, and Futaba Ohsaki for technical supports. I thank Drs. Kazuhisa Nakayama, Kazumasa Ohashi, and Shoji Yamaoka for kindly donating materials. This research was supported in part by the Japan Society for the Promotion of Science (JSPS) and Tohoku University Division for interdisciplinary Advanced Research and Education (DIARE). Finally, I would like to express my deep appreciation to all members of the Fukuda laboratory for share of fruitful research environment and friendly everyday conversation.